ELSEVIER

Biophysical Chemistry 94 (2001) 121–163

Biophysical Chemistry

www.elsevier.com/locate/bpc

Full-scale model of glycolysis in *Saccharomyces cerevisiae*

F. Hynne*, S. Danø, P.G. Sørensen

Department of Chemistry and CATS, H.C. Ørsted Institute, University of Copenhagen, Universitetsparken 5, DK-2100 Copenhagen, Denmark

Received 28 February 2001; received in revised form 11 September 2001; accepted 13 September 2001

Abstract

We present a powerful, general method of fitting a model of a biochemical pathway to experimental substrate concentrations and dynamical properties measured at a stationary state, when the mechanism is largely known but kinetic parameters are lacking. Rate constants and maximum velocities are calculated from the experimental data by simple algebra without integration of kinetic equations. Using this direct approach, we fit a comprehensive model of glycolysis and glycolytic oscillations in intact yeast cells to data measured on a suspension of living cells of *Saccharomyces cerevisiae* near a Hopf bifurcation, and to a large set of stationary concentrations and other data estimated from comparable batch experiments. The resulting model agrees with almost all experimentally known stationary concentrations and metabolic fluxes, with the frequency of oscillation and with the majority of other experimentally known kinetic and dynamical variables. The functional forms of the rate equations have not been optimized.

Keywords: Model of glycolysis; Glycolytic oscillations; Direct method of optimization; Reaction networks; Stationary state

1. Introduction

Glycolysis is at the heart of classical biochemistry and, as such, it has been thoroughly studied. When viewed as a collection of individual steps, it is very well described. When viewed as a whole, our understanding leaves much to be desired. A model assembled from mechanistic data alone will not reproduce any significant part of the experimental findings straight away; describing a complete pathway (including its dynamics) *quantitatively* requires a higher level of understanding in which delicate balances of different processes may become important. The recent work by Teusink et al. [1] illustrates some of the difficulties involved.

The purpose of this article is two-fold: to present a method which solves the problem of obtaining a realistic model of a biochemical pathway; and to use it for deriving a comprehensive model of glycolysis in a suspension of intact yeast cells, thus obtaining a full-scale model of glycolysis while demonstrating how the method is used in practice.

Traditional optimization methods integrate the kinetic equations with a trial set of parameters and selected initial conditions, and compare the result with experiments. If many kinetic parameters are unknown, searching for the right combination of

* Corresponding author. Tel.: +45-35-32-0225; fax: +45-35-32-0259.

E-mail address: fh@kiku.dk (F. Hynne).

0301-4622/01/$ - see front matter
PII: S0301-4622(01)00229-0

parameters is like looking for a needle in a haystack.

Our method can handle an entire pathway because it is efficient; it applies to a system in a stationary state and calculates mechanistic parameters like maximum velocities from substrate concentrations and metabolic fluxes without integration of kinetic equations. Thus, it inverts the traditional approach, and we refer to it as the direct method. It has been described before by Hynne et al. [2,3], but the practical approach to optimization for a biochemical pathway differs in a number of ways from that described previously. Therefore, we present the method with a view to its application in biochemical kinetics. We refer to Section 2.2 for a quick introduction to the essentials of the method.

Glycolytic oscillations in yeast cells provide a unique system for application of the direct method. Not only is the biochemistry of the pathway very well known, the biochemical and dynamical aspects of the oscillations are also well described from numerous experiments. In particular, we use experiments on sustained oscillations in non-growing cells of *Saccharomyces cerevisiae* in a flow reactor [4] and experiments performed by Westerhoff and co-workers (to be referred to as the Dutch group) [5–8] on the same system under comparable batch conditions.

Glycolytic oscillations have been modeled extensively in extracts. In broad terms, these models are either simple ones focusing on the dynamics of PFK[1] (e.g. [9,10]) or elaborate models encompassing most of the glycolytic reactions [11–14]. In particular, the models presented by Richter et al. [11] and by Nielsen et al. [14] both include the $NAD^+/NADH$ system. However, none of the yeast extract models include branching.

Modeling of glycolytic oscillations in intact yeast cells is somewhat more sparse. One reason for this might be the difficulties of using parameters obtained from in vitro studies for modeling an in vivo system. Often the V_{max} values of enzymes seem to be much higher in vivo than when they are measured in vitro (e.g. [1,15,16]). Several explanations have been offered for such phenomena (see, e.g. [17]). The direct method circumvents this problem since V_{max} parameters are not needed in the optimization.

It is potentially more interesting to model glycolysis in intact yeast cells because of the biotechnological importance of yeast. A good description of glycolytic oscillations could also increase our understanding of the cell synchronization observed experimentally in suspensions of yeast cells [6,18,19]. Qualitative [20,21] and semi-quantitative [22,23] models have been published which address the question of cell synchronization in yeast cells explicitly. Only a limited amount of biochemical detail has been incorporated in these models. See also refs. [24–26] for theoretical studies of synchronization.

Quantitative, full-scale models of glycolysis in intact yeast cells have previously been published [1,27]. These models have detailed biochemistry, including the $NAD^+/NADH$ system and branchings from glycolysis. In the work by Rizzi et al. [27], model parameters were fitted to the glucose response of yeast cells that were otherwise in steady state growth. Since the cells were growing, this model includes steady state fluxes from glycolysis to several other pathways. A reasonable agreement with the observed perturbation response was obtained through extensive fitting.

In the recent modeling work by the Dutch group [1], the fluxes and concentrations in a steady state, as well as a large number of enzyme kinetic parameters, are measured in non-growing, anaerobic yeast cells. The metabolite concentrations are then inserted into the equations of the model, and the calculated fluxes are compared with the experimental ones. Such a procedure has previously been described by Wurster and Schneider [28] and by Barwell and Hess [29], and similar calculations are discussed by Danø [30]. Despite the huge amount of high quality biochemical data considered, no actual optimization is performed. Neither Rizzi et al. nor Teusink et al. address glycolytic oscillations in their modeling.

The present article is essentially the completion of the work described by Danø [30]. Our use of the direct method enables us to include a wide range of biochemical and dynamical data in the optimization of a detailed biochemical model.

[1] See the list of abbreviations in Appendix A.

When setting up this model, we include only those reactions that are necessary for a meaningful comparison with all relevant experimental data. Because of the extensive set of data, we need a full-scale model; but we emphasize that completeness is not attempted for its own sake.

2. Conceptual basis

Because the approach described in the present paper has a number of unusual features, it may be helpful if we briefly outline the conceptual framework of the discussions to come. Throughout the paper, we shall try to present the work in biochemical terms as far as possible. However, to do justice to the rigorous, quantitative character of the underlying theory, we need some mathematics not part of classical biochemical kinetics. We shall explain the meaning of the various objects together with the notation in this section.

2.1. Definitions and notation

If a biochemical reaction system is specified through the set of kinetic equations with all kinetic parameters given, an instantaneous state of the system is given by a set of concentrations of all the metabolites. The concentration of species s is denoted c_s and is considered a component of a vector **c**. (For specific metabolites, the usual bracket notation is used, e.g. [G6P].) In biochemical systems, concentrations (activities) of enzymes are also important, but these may be considered part of the definition of the system as such rather than part of the state of the system (see Section 4 for a biochemical justification). Therefore, we will consider all enzyme concentrations fixed and, consequently, concentrations always refer to metabolites here. In the same way, the velocities of all the reactions in a given state are represented by a vector **v**, in which component v_r is the velocity of reaction r.

We shall model glycolysis in a suspension of intact yeast cells as a *two phase system* with one common, homogeneous, intracellular phase and one homogeneous extracellular phase, as we explain in Section 4. Because of the complication of two phases, we need to be careful with our definition of reaction velocity, so we first define the rate of conversion of reaction r as $\dot{\xi}_r$, the rate of change of the extent of reaction r. A dot denotes differentiation with respect to time. By definition, a change $\Delta\xi_r$, of the extent of reaction r results in a change of the amount n_s of species s equal to $\Delta n_s = \nu_{sr}\Delta\xi_r$, so that

$$\dot{n}_s = \sum_r \nu_{sr}\xi_r, \tag{1}$$

in which ν_{sr} is the stoichiometric coefficient of species s in reaction r, an element of the stoichiometric matrix $\boldsymbol{\nu}$.

It is convenient to define the rate of reaction r as $v_r = \dot{\xi}_r / V$ with V the total intracellular cytosol volume *regardless* of the character of the reaction (whether it is intracellular, extracellular, or it transfers some species across the membrane from one phase to the other). We denote the ratio of the extracellular volume to the total volume of intracellular cytosol by y_{vol}. We may then write Eq. (1) as

$$y_s\dot{c}_s = \sum_r \upsilon_{sr}v_r, \tag{2}$$

in which $y_s = y_{\mathrm{vol}}$, if s is extracellular and $y_s = 1$ for intracellular s.

It is straightforward to take the special definition of reaction velocities into account in the calculation of dynamical properties of the model (Section 5.2), in the calculation of rate constants and maximum velocities (Section 2.2), and in the integration of the final model (Section 8).

We shall be mostly concerned with stationary states in which concentrations and velocities are independent of time. Here, velocities are often handled conveniently in terms of net velocities (differences between forward and reverse velocities where appropriate). Net velocities form a vector **w**, which has a lower dimension than **v** if the reaction network has reversible steps. Any (net) stationary reaction velocity can be expressed in terms of (often just a few) special velocities with a simple biochemical interpretation. We shall explain this representation in biochemical terms in Section 5.1, see in particular, Eq. (5) which expresses a 24-dimensional net velocity in terms

of four special velocities related to branchings of the network.

2.2. Essentials of the direct method

The kinetics of a system can be described by the set of rate equations, each containing a set of parameters. This is the natural description when the kinetics is completely defined. However, we want to compare many different models of a system in a stationary state with concentrations **c**, so we need a more efficient way of defining a system. To explain the direct method, we first introduce some notation. The rate equations may be expressed as Eq. (2) together with expressions for the velocity v_r of each reaction r as a function of the concentration

$$v_r = \kappa_r g_r(\mathbf{c}, \mathbf{K}_r) \tag{3}$$

in which κ_r is the rate constant (if the reaction has mass–action kinetics) or the maximum velocity (for enzyme kinetics). The parameters κ_r may depend on enzyme concentrations, so it is convenient to distinguish them from the sets $\mathbf{K}_r$ of all other kinetic parameters (typically Michaelis constants). We refer to κ_r as a 'velocity parameter' and $\mathbf{K}_r$ as 'intrinsic parameters'.

Suppose the forms of all functions g_r are given and the set $\mathbf{K}_r$ of intrinsic parameters is known for each r. Then we can specify a model system and, at the same time, a stationary state of that system by a set of *stationary velocities,* **v** [satisfying Eq. (2) with zero left hand sides], together with *any* set of concentrations, **c**, which we want to become a stationary point.

This can be seen as follows. From such (**v**, **c**), we may obtain a set $\boldsymbol{\kappa}$ of all velocity parameters κ_r, from the set of Equation 3 by solving each equation separately for κ_r. Clearly, this set together with all the $\mathbf{K}_r$ defines a model completely. Moreover, that model has the chosen **c** as a stationary point by this construction since (reversing the argument) **c** for the model (with $\boldsymbol{\kappa}$) determines a **v** that implies $\dot{\mathbf{c}} = \mathbf{0}$ through Eq. (2). This is how the direct method defines a model system in a specific stationary state.

In the present work, we use pre-assigned forms for all the rate equations. So to fix a system and a stationary state for it, we need to specify a set of intrinsic parameters, $\mathbf{K}_r$ for all the reactions, a set of stationary velocities, **v**, and a set of stationary concentrations, **c**. We refer to the three sets together as a 'point'. If all parameters were known, these would determine a unique model, and no optimization would be needed. In practice, many parameters are incompletely known, so these parameters must be varied independently, while all known parameters are kept at their experimental values. In this search, the dynamical properties of each model (defined by a point) are calculated as described in Sections 2.3 and 5.2 and compared with experiments. The model that gives the best possible agreement is chosen as the result of the optimization.

We still need to explain how to get stationary reaction velocities. Briefly, we use a representation in terms of so-called extreme currents that are closely related to the branchings of the pathway. This is explained in Section 5.1 and Appendix B. There we show how all possible stationary reaction velocities can be easily generated. So we can easily generate 'all reasonable' systems in 'all reasonable' stationary states and compare their properties with experiments. This is exactly what we need for fitting a mechanism (parametrized model) to a set of data obtained experimentally for a stationary state.

2.3. Dynamics

The dynamical behavior of a stationary state is very simple because its state does not change with time. In contrast, an oscillating state is much more expressive as regards dynamical properties. We may get the rich dynamics of an oscillatory system *while retaining* the simplicity of a stationary state if we work at (or near) a Hopf bifurcation, which we now briefly explain.

A bifurcation is a change of qualitative behavior of solutions to a differential equation when a parameter is changed. In particular, a supercritical Hopf bifurcation is the onset of oscillations when a stable stationary state becomes unstable and sustained oscillations appear. The stable oscillations of constant amplitude are associated with a 'limit cycle' in the concentration space (explained

below). At a supercritical Hopf bifurcation, the amplitude of the limit cycle oscillations grows continuously from zero (at the bifurcation point) as some parameter is changed. At the bifurcation point we, in a sense, *have a stationary state and an oscillatory state at the same time*. This situation is ideal for optimization of a model. We shall use the term Hopf bifurcation without qualification to mean a supercritical Hopf bifurcation. (There also exist subcritical bifurcations which we need not worry about in this paper except that we must make sure that the bifurcations we consider in the model are in fact supercritical, a question discussed in Appendix C.)

Beyond a Hopf bifurcation, all concentrations show sinusoidal oscillations with the same frequency and constant amplitudes, which can be described as a point circulating a (small) closed curve in concentration space, a limit cycle. (The name indicates the property that any state close enough to the curve will approach the closed curve in the course of time.) The behavior of a system near a Hopf bifurcation is universal (common to any system in any Hopf bifurcation). For example, the small closed curve is almost planar and has elliptic shape, and it grows in size with almost constant proportions and orientation in space as a parameter (μ say) is changed beyond the bifurcation (at μ_0). In fact, its size grows as the square root of the distance from the bifurcation point, i.e. as $\sqrt{(\mu-\mu_0)}$ if the stable oscillations arise for $\mu > \mu_0$. This means that the square of the amplitude grows linearly with $(\mu > \mu_0)$. Close to the bifurcation points, Fig. 1a,b and Fig. 7a demonstrate this dependence of the amplitude on the mixed flow glucose concentration (Fig. 7a) and mixed flow cyanide concentration (Fig. 1a,b) observed in experiments with suspensions of living yeast cells, described in Section 3.

2.4. Connection with experiments

The simple geometry of a small elliptic limit cycle and other features of the dynamics, characteristic of a Hopf bifurcation, can be utilized to get kinetically relevant information about the system. The dynamical behavior of a system near any

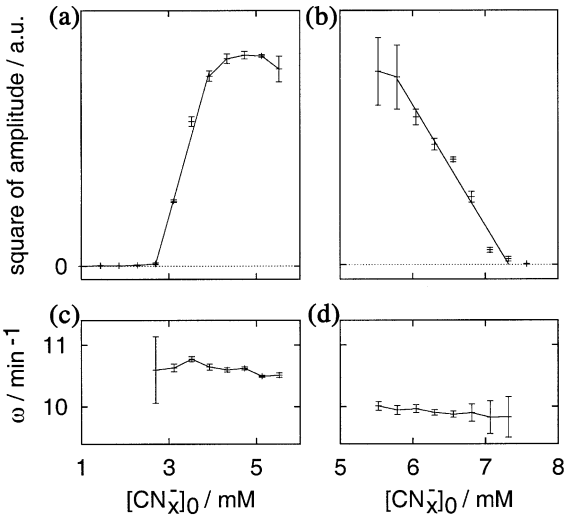

Fig. 1. Square of amplitude as functions of the mixed flow cyanide concentration $[CN_x^-]_0$ in (a) the low end, and (b) the high end. Panels (c) and (d) show the corresponding variation of the angular frequency. In (a) and (c), the cell density, the mixed flow glucose concentration $[Glc_x]_0$, and the specific flow rate k_0 were fixed at 1.64×10^9 cells/ml, 28 mM, and 0.048 min^{-1}, respectively. In (b) and (d), these parameters were 1.61×10^9 cells/ml, 27 mM, and 0.050 min^{-1}, respectively. The abbreviation a.u. means arbitrary units (see Danø [30] for further details.)

stationary point can be described quite accurately by the kinetics, linearized about the stationary state, embodied in the Jacobi matrix, **J**,

$$\dot{c}_s \approx \sum_p J_{sp}(c_p - c_p^*). \tag{4}$$

Here c_p^* denotes the stationary concentration of species p, and J_{sp} is an element of the Jacobi matrix, discussed in Section 5.2.

The relative amplitudes and phases of the concentration oscillations of the various species can sometimes be measured and can easily be calculated from the Jacobi matrix for a model. At a Hopf bifurcation, **J** has a pair of pure imaginary eigenvalues, $\pm i\omega_0$, where ω_0 is the angular frequency of the emerging oscillations. Suitably normalized, the right eigenvector associated with the eigenvalue $-i\omega_0$ has a complex component $a_s \exp(i\theta_s)$ for species s, for which the modulus, a_s is the relative amplitude, and the argument, θ_s, is the relative phase of the small amplitude oscilla-

tions of c_s near the bifurcation [31]. The eigenvector can be normalized so that amplitudes and phases are relative to those of a selected species. (We shall use [NADH] as a reference for glycolysis.)

The pair of left eigenvectors of **J** corresponding to the eigenvalues $\pm i\omega_0$, can also be calculated and can in fact, be measured experimentally through special perturbation experiments; small sinusoidal oscillations just beyond a Hopf bifurcation can be temporarily stopped ('quenched') by addition of a specific amount of a relevant species in a specific phase of the oscillations.

For a given species, s, the unique change of concentration by the addition, q_s, and the unique quenching phase, ϕ_s, together determine the s-component of the left eigenvector corresponding to the eigenvalue $i\omega_0$, for that species as $-\exp(i\phi_s)/q_s$, relative to the same reference as for the oscillation amplitude and phase [31]. Thus, quenching experiments can provide data useful for optimizing a model.

What happens in a quenching experiment can be understood geometrically [31]. Briefly, the representative point in concentration space is shifted from its instantaneous position on the limit cycle to the unstable stationary point by the addition of the species and subsequent (fast) chemical reactions. Here, the system shows no oscillations (because it is in a stationary state), but because the state is unstable, the system will slowly return to the limit cycle oscillations. (The fast chemical reactions referred to can also be understood geometrically in terms of the 'stable manifold' of the unstable stationary point, as explained by Hynne et al. [31].)

2.5. Non-linearities

To describe the behavior of the oscillatory modes near a Hopf bifurcation including the limit cycle and its dependence on a bifurcation parameter, it is necessary to include also non-linear terms for these modes. (For all the other modes, the linear approximation is usually sufficient.) Such more adequate treatment is best made through a normal form description. Here, the oscillations are described in simplified form through an amplitude equation (a scaled or unscaled normal form equation), which is sufficient to determine whether the bifurcation is supercritical or subcritical and to calculate a bifurcation diagram showing how fast the amplitude of the limit cycle oscillations grows and the frequency changes with a bifurcation parameter. These properties can be expressed succinctly through certain normal form parameters, g', g'', σ' and σ'', that can also be determined experimentally. They are discussed in Appendix C and are included in the comparisons in Section 7.

The fully developed normal form theory can also provide a transformation from amplitudes to concentrations so that we may find the actual behavior of each of the metabolites including shift of the (unstable) stationary state and the anharmonicity of the oscillations. We summarize the results of the theory and present the parameters for the glycolytic model in Appendix C.

3. Experimental basis

The model derived in this paper is based on two categories of experimental data. First of all we build on results of extensive biochemical studies, often focussed on particular reactions, to set up the network of reactions and associated rate expressions for a full-scale model of glycolysis in intact yeast cells. The functional forms of the rate expressions have been determined by classical biochemical methods, and many of the kinetic parameters in the expressions have been determined experimentally in these previous studies; but others are unknown or have merely been estimated. The set of reactions and rate expressions used in the model is described in the next section.

The other category of experimental data used for the modeling applies to the complete system in a definite state, and so expresses properties of the full biochemical pathway in that state. These data include a complete 'external' specification of the state of the system (the operating point) as well as results of biochemical and dynamical measurements on the system in that state. The data obtained from these experiments help us select the set of parameters for the rate expressions for which the properties of the model agree best with avail-

able experiments. These underlying experiments are described in this section.

3.1. CSTR experiments

The specific situation, which we model, is the set-up used for measuring dynamical properties of intact yeast cells [4]. These measurements were performed in a continuous-flow stirred tank reactor (CSTR) in which glucose, cyanide, and a suspension of starved yeast cells flow into the reactor at a constant rate, and surplus liquid is removed to maintain a fixed volume. This way, the system can be maintained indefinitely in a well-defined stationary or oscillatory (limit cycle) state, and by changing the flowrates, we can investigate many different states. The cell suspension consists of yeast cells (*Saccharomyces cerevisiae*) grown in a batch culture to the point of glucose depletion, washed, starved, and placed in a phosphate buffer as described by Richard et al. [7,32]. During the CSTR experiments, we monitor the cell population by measuring the NADH autofluorescence of the yeast cells.

A key parameter here is the ratio, y_{vol}, of the extracellular volume to the cytosolic volume. This ratio is inversely proportional to the cell density, and the conversion factor between cell density (measured either as wet weight or as protein mass per volume), and y_{vol} is given in Richard et al. [7]. We tried to use these conversion factors to determine y_{vol} for the CSTR experiments, but the two conversion factors give inconsistent results. Therefore, we have no accurate value for y_{vol}. For future reference, we have determined the dry weight of the cell suspension defining the working point of the optimization to 30.5 mg/ml (equivalent to 1.61×10^9 cells/ml).

An important feature of the present optimization is that it is made at a Hopf bifurcation, where a stable steady state becomes unstable and oscillations emerge. Using the CSTR set-up, it is possible to measure the exact location of bifurcations. With a constant mixed flow concentration, $[CN_x^-]_0 = 5.60$ mM, of CN_x^-, and the mixed flow glucose concentration, $[Glc_x]_0$, as a bifurcation parameter, we found a bifurcation at $[Glc_x]_0 = 18.5$ mM (Fig. 7a; [4]), corresponding to an extracellular glucose concentration of 1.6 mM. This bifurcation point defines our exact reference point of the optimization; the operating conditions for this point, listed in Tables 1–7, form an important part of the experimental data set, which the model should agree with. The frequency of the oscillations at the bifurcation is determined accurately by extrapolation (see Fig. 7b).

Table 1
Reactions of the model

r		Reaction
1	inGlc	$\rightleftharpoons Glc_x$
2	GlcTrans	$Glc_x \rightleftharpoons Glc$
3	HK	$Glc + ATP \rightarrow G6P + ADP$
4	PGI	$G6P \rightleftharpoons F6P$
5	PFK	$F6P + ATP \rightleftharpoons FBP + ADP$
6	ALD	$FBP \rightleftharpoons GAP + DHAP$
7	TIM	$DHAP \rightleftharpoons GAP$
8	GAPDH	$GAP + NAD^+ \rightleftharpoons BPG + NADH$
9	lpPEP	$BPG + ADP \rightleftharpoons PEP + ATP$
10	PK	$PEP + ADP \rightarrow Pyr + ATP$
11	PDC	$Pyr \rightarrow ACA$
12	ADH	$ACA + NADH \rightarrow EtOH + NAD^+$
13	difEtOH	$EtOH \rightleftharpoons EtOH_x$
14	outEtOH	$EtOH_x \rightarrow$
15	lpGlyc	$DHAP + NADH \rightarrow Glyc + NAD^+$
16	difGlyc	$Glyc \rightleftharpoons Glyc_x$
17	outGlyc	$Glyc_x \rightarrow$
18	difACA	$ACA \rightleftharpoons ACA_x$
19	outACA	$ACA_x \rightarrow$
20	lacto	$ACA_x + CN_x^- \rightarrow$
21	inCN	$CN_x^- \rightleftharpoons$
22	storage	$G6P + ATP \rightarrow ADP$
23	consum	$ATP \rightarrow ADP$
24	AK	$ATP + AMP \rightleftharpoons 2\ ADP$

$[NAD^+] + [NADH] =$ constant, and
$[ATP] + [ADP] + [AMP] =$ constant.

Important dynamical properties of the system are obtained by quenching the oscillations, the special perturbations mentioned in Section 2. In the experiments [4] we found that the oscillating suspension of yeast cells can be quenched with extracellular acetaldehyde and — close enough to the bifurcation point at low glucose concentrations — with extracellular glucose (Table 6). Quenchings of the oscillations with other extracellular species: ethanol; pyruvate; glycerol (this study); and cyanide were not possible. As mentioned in Section 2, the quenching concentrations and quenching phases for addition of extracellular acet-

Table 2
The rate equations of the model (for mechanistic details and the significance of the parameters, see the references given in the last column)

r	Rate equation (v_r)	Refs.
1	$v_{\rightarrow} = y_{vol} k_0 [Glc_x]_0$ $v_{\leftarrow} = y_{vol} k_0 [Glc_x]$	
2	$v_{\rightarrow} = \dfrac{V_{2m}\dfrac{[Glc_x]}{K_{2Glc}}}{1+\dfrac{[Glc_x]}{K_{2Glc}}+\dfrac{P_2\dfrac{[Glc_x]}{K_{2Glc}}+1}{P_2\dfrac{[Glc]}{K_{2Glc}}+1}\left(1+\dfrac{[Glc]}{K_{2Glc}}+\dfrac{[G6P]}{K_{2IG6P}}+\dfrac{[Glc][G6P]}{K_{2Glc}K_{2IIG6P}}\right)}$ $v_{\leftarrow} = \dfrac{V_{2m}\dfrac{[Glc]}{K_{2Glc}}}{1+\dfrac{[Glc]}{K_{2Glc}}+\dfrac{P_2\dfrac{[Glc]}{K_{2Glc}}+1}{P_2\dfrac{[Glc_x]}{K_{2Glc}}+1}\left(1+\dfrac{[Glc_x]}{K_{2Glc}}\right)+\dfrac{[G6P]}{K_{2IG6P}}+\dfrac{[Glc][G6P]}{K_{2Glc}K_{2IIG6P}}}$	[44]
3	$v_{\rightarrow} = \dfrac{V_{3m}[ATP][Glc]}{K_{3DGlc}K_{3ATP}+K_{3Glc}[ATP]+K_{3ATP}[Glc]+[Glc][ATP]}$	[46,62]
4	$v_{\rightarrow} = \dfrac{V_{4m}[G6P]}{K_{4G6P}+[G6P]+\dfrac{K_{4G6P}}{K_{4F6P}}[F6P]}$ $v_{\leftarrow} = \dfrac{V_{4m}\dfrac{[F6P]}{K_{4eq}}}{K_{4G6P}+[G6P]+\dfrac{K_{4G6P}}{K_{4F6P}}[F6P]}$	[11]
5	$v_{\rightarrow} = \dfrac{V_{5m}[F6P]^2}{K_5\left(1+\kappa_5\dfrac{[ATP]^2}{[AMP]^2}\right)+[F6P]^2}$	[12]
6	$v_{\rightarrow} = \dfrac{V_{6f}[FBP]}{K_{6FBP}+[FBP]+\dfrac{[GAP]K_{6DHAP}V_{6f}}{K_{6eq}V_{6r}}+\dfrac{[DHAP]K_{6GAP}V_{6f}}{K_{6eq}V_{6r}}+\dfrac{[FBP][GAP]}{K_{6IGAP}}+\dfrac{[GAP][DHAP]V_{6f}}{K_{6eq}V_{6r}}}$ $v_{\leftarrow} = \dfrac{V_{6f}\dfrac{[GAP][DHAP]}{K_{6eq}}}{K_{6FBP}+[FBP]+\dfrac{[GAP]K_{6DHAP}V_{6f}}{K_{6eq}V_{6r}}+\dfrac{[DHAP]K_{6GAP}V_{6f}}{K_{6eq}V_{6r}}+\dfrac{[FBP][GAP]}{K_{6IGAP}}+\dfrac{[GAP][DHAP]V_{6f}}{K_{6eq}V_{6r}}}$	[11,46]
7	$v_{\rightarrow} = \dfrac{V_{7m}[DHAP]}{K_{7DHAP}+[DHAP]+\dfrac{K_{7DHAP}}{K_{7GAP}}[GAP]}$ $v_{\leftarrow} = \dfrac{V_{7m}\dfrac{[GAP]}{K_{7eq}}}{K_{7DHAP}+[DHAP]+\dfrac{K_{7DHAP}}{K_{7GAP}}[GAP]}$	[11]

Table 2 *Continued*

r	Rate equation (v_r)	Refs.
8	$v_{\rightarrow} = \dfrac{V_{8m}[\mathrm{GAP}][\mathrm{NAD}^+]}{K_{8\mathrm{GAP}}K_{8\mathrm{NAD}}\left(1+\dfrac{[\mathrm{GAP}]}{K_{8\mathrm{GAP}}}+\dfrac{[\mathrm{BPG}]}{K_{8\mathrm{BPG}}}\right)\left(1+\dfrac{[\mathrm{NAD}^+]}{K_{8\mathrm{NAD}}}+\dfrac{[\mathrm{NADH}]}{K_{8\mathrm{NADH}}}\right)}$ $v_{\leftarrow} = \dfrac{V_{8m}\dfrac{[\mathrm{BPG}][\mathrm{NADH}]}{K_{8eq}}}{K_{8\mathrm{GAP}}K_{8\mathrm{NAD}}\left(1+\dfrac{[\mathrm{GAP}]}{K_{8\mathrm{GAP}}}+\dfrac{[\mathrm{BPG}]}{K_{8\mathrm{BPG}}}\right)\left(1+\dfrac{[\mathrm{NAD}^+]}{K_{8\mathrm{NAD}}}+\dfrac{[\mathrm{NADH}]}{K_{8\mathrm{NADH}}}\right)}$	[1]
9	$v_{\rightarrow} = k_{9f}[\mathrm{BPG}][\mathrm{ADP}]$ $v_{\leftarrow} = k_{9r}[\mathrm{PEP}][\mathrm{ATP}]$	
10	$v_{\rightarrow} = \dfrac{V_{10m}[\mathrm{ADP}][\mathrm{PEP}]}{(K_{10\mathrm{PEP}}+[\mathrm{PEP}])(K_{10\mathrm{ADP}}+[\mathrm{ADP}])}$	[46]
11	$v_{\rightarrow} = \dfrac{V_{11m}[\mathrm{Pyr}]}{K_{11}+[\mathrm{Pyr}]}$	
12	$v_{\rightarrow} = \dfrac{V_{12m}[\mathrm{ACA}][\mathrm{NADH}]}{(K_{12\mathrm{NADH}}+[\mathrm{NADH}])(K_{12\mathrm{ACA}}+[\mathrm{ACA}])}$	[46]
13	$v_{\rightarrow} = k_{13}[\mathrm{EtOH}]$ $v_{\leftarrow} = k_{13}[\mathrm{EtOH}_x]$	
14	$v_{\rightarrow} = y_{\mathrm{vol}}k_0[\mathrm{EtOH}_x]$	
15	$v_{\rightarrow} = \dfrac{V_{15m}[\mathrm{DHAP}]}{K_{15\mathrm{DHAP}}\left(1+\dfrac{K_{15\mathrm{INADH}}}{[\mathrm{NADH}]}\left(1+\dfrac{[\mathrm{NAD}^+]}{K_{15\mathrm{INAD}}}\right)\right)+[\mathrm{DHAP}]\left(1+\dfrac{K_{15\mathrm{NADH}}}{[\mathrm{NADH}]}\left(1+\dfrac{[\mathrm{NAD}^+]}{K_{15\mathrm{INAD}}}\right)\right)}$	[45]
16	$v_{\rightarrow} = k_{16}[\mathrm{Glyc}]$ $v_{\leftarrow} = k_{16}[\mathrm{Glyc}_x]$	
17	$v_{\rightarrow} = y_{\mathrm{vol}}k_0[\mathrm{Glyc}_x]$	
18	$v_{\rightarrow} = k_{18}[\mathrm{ACA}]$ $v_{\leftarrow} = k_{18}[\mathrm{ACA}_x]$	
19	$v_{\rightarrow} = y_{\mathrm{vol}}k_0[\mathrm{ACA}_x]$	
20	$v_{\rightarrow} = y_{\mathrm{vol}}k_{20}[\mathrm{ACA}_x][\mathrm{CN}_x^-]$	
21	$v_{\rightarrow} = y_{\mathrm{vol}}k_0[\mathrm{CN}_x^-]_0$ $v_{\leftarrow} = y_{\mathrm{vol}}k_0[\mathrm{CN}_x^-]$	
22	$v_{\rightarrow} = k_{22}[\mathrm{ATP}][\mathrm{G6P}]$	
23	$v_{\rightarrow} = k_{23}[\mathrm{ATP}]$	
24	$v_{\rightarrow} = k_{24f}[\mathrm{AMP}][\mathrm{ATP}]$ $v_{\leftarrow} = k_{24r}[\mathrm{ADP}]^2$	

aldehyde and glucose can also be calculated from a left eigenvector in a model and compared with the experimental values as part of the optimization.

The quenchings must necessarily be carried out in a region of sinusoidal oscillations with small but non-zero amplitude. The actual operating

Table 3
Extreme currents based on velocities defined near Eq. (2), compared with Fig. 3

r	React	$\mathbf{E}_{\mathrm{ferm}}/v_0$	$\mathbf{E}_{\mathrm{glyc}}/v_0$	$\mathbf{E}_{\mathrm{lact}}/v_0$	$\mathbf{E}_{\mathrm{stor}}/v_0$
1	inGlc	1	1	1	2
2	GlcTrans	1	1	1	2
3	HK	1	1	1	2
4	PGI	1	1	1	1
5	PFK	1	1	1	1
6	ALD	1	1	1	1
7	TIM	1	0	0	1
8	GAPDH	2	1	1	2
9	lpPEP	2	1	1	2
10	PK	2	1	1	2
11	PDC	2	1	1	2
12	ADH	2	0	0	2
13	difEtOH	2	0	0	2
14	outEtOH	2	0	0	2
15	lpGlyc	0	1	1	0
16	difGlyc	0	1	1	0
17	outGlyc	0	1	1	0
18	difACA	0	1	1	0
19	outACA	0	1	0	0
20	lacto	0	0	1	0
21	inCN	0	0	1	0
22	storage	0	0	0	1
23	consum	2	0	0	0
24	AK	0	0	0	0

points used for the perturbation experiments were different for the glucose perturbation and the acetaldehyde perturbation, as noted in Danø et al. [4] and Fig. 10[2]. However, when scaled by the amplitude of the limit cycle oscillations, the quenching data are independent of the distance from the bifurcation point to a good approximation, and can be compared with data for a model calculated at the bifurcation point. This fact follows from the quenching theory [31] and the theory behind the Hopf bifurction [33] (see also Ipsen et al. [34]).

When the mixed flow glucose concentration is increased well beyond the operating point for the perturbation experiment for glucose, the yeast cells become insensitive to glucose perturbations, and the amplitude and frequency of the oscillations become almost independent of the glucose flow rate. Also, the waveform remains almost sinusoidal. We have interpreted this behavior as saturation of the glucose transporter. As explained in Section 3.2, this interpretation is supported by biochemical measurements. In Section 8 where we study the model developed in this paper by integration of the kinetic equations, we shall see that it exhibits glucose saturation as well.

The saturation of the glucose transporter has the effect that the yeast cells can never be taken far away from the Hopf bifurcation by increasing the mixed flow glucose concentration. Therefore, the cells retain the universal near-Hopf behavior even for high values of $[\mathrm{Glc}_x]_0$, and more complex dynamics are not found in the system treated here — despite the fact that complex oscillations and chaos have been observed in yeast extracts [35]. Consequently, the simple Hopf normal form description of the system (see Appendix C) is useful under a wide range of operating conditions (i.e. of $[\mathrm{Glc}_x]_0$). For example, Fig. 10 in Appendix C shows that two quenching experiments can be fitted using the same normal form parameters even though they are performed at different mixed flow glucose concentrations (23.1 and 35.0 mM for the Glc_x and the ACA_x quenching, respectively).

When the mixed flow concentration of glucose is kept constant near 28 mM and the mixed flow cyanide concentration is used as a bifurcation parameter, we find bifurcations at low and high cyanide concentrations with oscillations at intermediate concentrations (Fig. 1).

By fitting an extended normal form expression to the time series of a quenching event, we can also obtain experimental estimates of normal form parameters, as discussed in Appendix C.

3.2. Batch experiments

The measurements of dynamical properties just described are complemented by a large set of biochemical measurements (some featuring dynamical properties) performed by the Dutch group [5–8]. This series of experiments was made with the same strain of yeast as that used in the CSTR experiments, and the yeast was grown, harvested and starved in the same way. However, the experiments were made in batch where a pulse of glucose and subsequently, a pulse of cyanide were added to a cell suspension in an otherwise closed reactor. Although the conditions of these

[2] In Appendix C.

Table 4
Calculated maximum velocities and rate constants

r	Reaction	Parameter	Forward	Reverse
1	inGlc	k_0 (min^{-1})	0.048	0.048
2	GlcTrans	V_{2m} ($mM\ min^{-1}$)	1.01496×10^{3}	1.01496×10^{3}
3	HK	V_{3m} ($mM\ min^{-1}$)	5.17547×10^{1}	
4	PGI	V_{4m} ($mM\ min^{-1}$)	4.96042×10^{2}	4.96042×10^{2}
5	PFK	V_{5m} ($mM\ min^{-1}$)	4.54327×10^{1}	
6	ALD	V_{6m} ($mM\ min^{-1}$)	2.20782×10^{3}	1.10391×10^{4}
7	TIM	V_{7m} ($mM\ min^{-1}$)	1.16365×10^{2}	1.16365×10^{2}
8	GAPDH	V_{8m} ($mM\ min^{-1}$)	8.33858×10^{2}	8.33858×10^{2}
9	lpPEP	k_9 ($mM^{-1}\ min^{-1}$)	4.43866×10^{5}	1.52862×10^{3}
10	PK	V_{10m} ($mM\ min^{-1}$)	3.43096×10^{2}	
11	PDC	V_{11m} ($mM\ min^{-1}$)	5.31328×10^{1}	
12	ADH	V_{12m} ($mM\ min^{-1}$)	8.98023×10^{1}	
13	difEtOH	k_{13} (min^{-1})	1.67200×10^{1}	1.67200×10^{1}
14	outEtOH	k_0 (min^{-1})	0.048	
15	lpGlyc	V_{15m} ($mM\ min^{-1}$)	8.14797×10^{1}	
16	difGlyc	k_{16} (min^{-1})	1.9	1.9
17	outGlyc	k_0 (min^{-1})	0.048	
18	difACA	k_{18} (min^{-1})	2.47×10^{1}	2.47×10^{1}
19	outACA	k_0 (min^{-1})	0.048	
20	lacto	k_{20} ($mM^{-1}\ min^{-1}$)	2.83828×10^{-3}	
21	inCN	k_0 (min^{-1})	0.048	0.048
22	storage	k_{22} ($mM^{-1}\ min^{-1}$)	2.25932	
23	consum	k_{23} (min^{-1})	3.20760	
24	AK	k_{24} ($mM\ min^{-1}$)	4.32900×10^{2}	1.33333×10^{2}

For extracellular reactions, the values have been corrected (by y_{vol}) so that they refer to the extracellular volume (all parameters are accurate to six significant digits, see Section 6).

batch experiments differ from those of the CSTR experiments we are trying to model, we include the results in the set of experimental data used for the optimization with the following justification.

Calorimetric measurements [8] indicate that when the cells are harvested at the point of glucose depletion or later, then the average glycolytic flux remains approximately constant during the oscillations. A reason for this could be that the glucose transporter is saturated, and therefore, the glucose flux into the cells stays nearly constant even though the extracellular glucose concentration is changing. This interpretation agrees well with the change of glucose transport affinity during growth on glucose (see, e.g. the K_M values in Teusink et al. [36]) and with the results presented in refs. [37,38]. It also agrees with the indications from the CSTR experiments of glucose transporter saturation (Section 3.1).

In this sense, the specific make-up of the cells sets up an approximately constant flow of glucose into the cells even in the batch experiments. Therefore, it seems reasonable to include results from the Dutch batch experiments with the results from the CSTR experiments in the optimization, at least for intracellular species. (For extracellular species, we must expect differences depending on the precise sampling in the batch experiments vs. the residence time in the CSTR.) Because the glucose bifurcation is most likely to be a supercritical Hopf bifurcation in each of the cells (Section 4 and Danø et al. [4]), and since the saturation happens close to the glucose bifurcation point (Fig. 7a), mean values of oscillating metabolite concentrations from the batch experiments are good approximations to the steady state concentrations at the bifurcation point. Likewise, these experiments can be used to estimate the metabolic fluxes of the system.

This way, the experiments reported in Richard et al. [6,7] provide data on 12 quasistationary

Table 5
Comparison with literature: intrinsic parameters (defined in Table 2); literature values in parentheses are parameters from other models, which are cited because no biochemical data are available

Reaction	Parameter	Model	Literature	Reference
GlcTrans	$K_{2\mathrm{Glc}}$	1.7	1.1, 1.7	[63,36]
	$K_{2\mathrm{IGGP}}$	1.2	1.2	[44]
	$K_{2\mathrm{IGGP}}$	7.2	7.2	[44]
	P_2	1	1, 1.87	Most plausible value, [64]
HK	$K_{3\mathrm{ATP}}$	0.1	0.1, 0.15[a], 0.2[b]	[65–67]
			0.29[a], 0.3[b]	[67,67]
	$K_{3\mathrm{Glc}}$	0	0.1, 0.12[b], 0.12[a], 0.12[b]	[65,68,68,66]
			0.23[a], 0.2–0.3[b], 0.25–0.6[a]	[66,67,67]
	$K_{3\mathrm{dGlc}}$	0.37		
PGI	$K_{4\mathrm{G6P}}$	0.8	0.27, 0.3, 0.7, 0.8, 1.5	[69]
	$K_{4\mathrm{F6P}}$	0.15	0.11, 0.15, 0.23	[69]
	K_{4eq}	0.13	0.3	[70,71]
PFK	K_5	0.021	(0.0016)	[14]
	K_5	0.15	(0.0017)	[14]
ALD	V_{6r}/V_{6f}	5	(5)	[11]
	K_{6eq}	0.081	0.08, 0.081	[72,73]
	$K_{6\mathrm{FBP}}$	0.3	(0.3)	[11]
	$K_{6\mathrm{GAP}}$	4.0	(2.0)	[11]
	$K_{6\mathrm{DHAP}}$	2.0	(2.0)	[11]
	$K_{6\mathrm{IGAP}}$	10.0	(10.0)	[11]
TIM	$K_{7\mathrm{DHAP}}$	1.23	1.23	[74]
	$K_{7\mathrm{GAP}}$	1.27	1.27	[74]
	K_{7eq}	0.055	0.045[c]	[70]
GAPDH	$K_{8\mathrm{GAP}}$	0.6	0.6	[75]
	$K_{8\mathrm{BPG}}$	0.01		
	$K_{8\mathrm{NAD}}$	0.1	0.1	[75]
	$K_{8\mathrm{NADH}}$	0.06		
	K_{8eq}	0.0055[d]	0.0055[d]	[76]
PK	$K_{10\mathrm{ADP}}$	0.17	0.16–0.17, 0.36	[69,29]
	$K_{10\mathrm{PEP}}$	0.2	0.099, 0.2	[77,29]
PDC	K_{11}	0.3	(0.3)	[14]
ADH	$K_{12\mathrm{ACA}}$	0.71	0.84, 0.93, 1.1[e]	[78–80]
	$K_{12\mathrm{NADH}}$	0.1	0.084, 0.096, 0.110[e]	[78–80]
difEtOH	k_{13}	$k_{16}\times 8.8$	$k_{16}\times 8.8$[f]	[49]
G3PDH	$K_{15\mathrm{NADH}}$	0.13	0.13, 0.023, 0.016–0.027	[45,81,69]
	$K_{15\mathrm{DHAP}}$	25	0.54[g], 1.6[g]	[81,45]
	$K_{15\mathrm{INADH}}$	0.034	0.034	[45]
	$K_{15\mathrm{INAD}}$	0.13	0.13, 0.93	[45,81]
difGlyc	k_{16}	1.9		
difACA	k_{18}	$k_{16}\times 13$	$k_{16}\times 13$[f]	[49]

[a] Isozyme PII.
[b] Isozyme PI.
[c] This equilibrium constant is inconsistent with the measurements of metabolite concentrations [7] and metabolic fluxes [5].
[d] Apparent equilibrium constant with the concentration of inorganic phosphate fixed at the mean value of 11 mM reported in Richard et al. [7].
[e] Isozyme I.
[f] Based on empirical formulas for partitioning coefficients.
[g] The apparent value of $K_{15\mathrm{DHAP}}$ will be significantly higher due to the presence of inorganic phosphate [45].
Conditions: 25 °C and pH = 7.0 where possible.

Table 6
Comparison with experiments related to metabolites

s	c_s (mM)		a_s/a		θ_s (°)		q_s/a		ϕ_s (°)	
	Mod[a]	Exp	Mod	Exp[c]	Mod	Exp	Mod	Exp	Mod	Exp
Glc_x	1.55307	1.6	0.013		135		65.7	1.11 mM/a	−5	4
Glc	0.573074		1.83		12		223		81	
G6P	4.2	4.1	15.8	21	−170	−100	20.6		67	
F6P	0.49	0.5	2.16	2.7	178	−110	20.6		72	
FBP	4.64	5.1	22.2	26	32	70	54.0		−142	
GAP	0.115	0.12	0.295	0.04	30		86.7		−105	
DHAP	2.95	2.5	6.97	0.5	38		98.5		−165	
BPG	0.00027	n.d.[e]	0.002		136		6.63		−73	
PEP	0.04	0.04	0.023	0.07	18		13.6		−74	
Pyr	8.7	8.7	4.06	7	79		1550		180	
ACA	1.48153		0.894		−164		30.4		−92	
EtOH	19.2379		1.22		26		∞		Undef	
$EtOH_x$	16.4514	7.1[b]	0.035		114		∞	Impossible[d]	Undef	
Glyc	4.196		1.68		98		∞		Undef	
$Glyc_x$	1.68478	1.3[b]	0.005		−172		∞	Impossible[d]	Undef	
ACA_x	1.28836	0.07[b]	0.037	0.3	−76	−160	12.4	98 μM/a	−179	172
CN_x^-	5.20358		5×10^{-5}		−167		3×10^4	Impossible[d]	−89	
ATP	2.1	2.1	10.8	8	139	180	6.22		−71	
ADP	1.5	1.5	6.32	9.4	−41	0	12.3		−70	
AMP	0.33	0.33	4.5	3.6	−41	0				
NADH	0.33	0.33	1	1	0	0	8.48		106	
NAD^+	0.65	0.65	1	0.6	180	180				

[a] All model concentrations are accurate to six significant digits, see Section 6.
[b] In batch; not directly comparable with CSTR results for extracellular metabolites.
[c] See Section 3 for a discussion of the experimental amplitudes.
[d] Quenching was attempted but was not possible. This corresponds to a high value of q_s/a.
[e] n.d.: not detectable.

Concentrations c_s of species s. Oscillation amplitude a_s in units of the NADH amplitude a. Oscillation phase θ_s in degrees relative to the oscillation phase of NADH. Quenching concentration q_s in units of a. Quenching phase θ_s in degrees relative to the oscillation phase of NADH. Experimental data are from refs. [4–7] as described in text, and from this study. Note that angles are quoted in the interval from −180 to +180° by convention. Thus, −180 and +180° represent the same angle.

concentrations, 13 amplitudes and nine relative phases of metabolites, reproduced in Table 6.

It is known that the starvation of the yeast cells is essential for the appearance of glycolytic oscillations [38]. Probably, the reason for this is that starved cells build a substantial part of the glucose taken up into glycogen. This should be taken into account when estimating the metabolic fluxes.

Table 7
Comparison with experiments: operating point (experimental data from refs. [4,5,7] as described in text)

	Parameter	Model	Exp.
Volume ratio	y_{vol}	59	∼45[a]
Specific flow rate at bifurcation	k_0 (min^{-1})	0.048	0.048
Mixed flow concentration, glucose	$[Glc_x]_0$ (mM)	18.5	18.5
Mixed flow concentration, cyanide	$[CN_x^-]_0$ (mM)	5.60	5.60
Glycolytic flux	$j_0 v_0$ (mM min^{-1})	28	27
Cellular glucose uptake rate	k_0 ($[Glc_x]_0-[Glc_x]$)y_{vol} (mM min^{-1})	48	

[a] See comment in Section 3.

Table 8
Comparison with experiments: branching of glycolysis in terms of normalized convex coefficients, see Eqs. (5) and (6); (experimental data from refs. [5,39] as described in Section 3.2 and [30])

Branch	Convex coefficient	Model	Exp.
Glycolysis and fermentation	j_{ferm}	0.12	0.12
Glycerol production	j_{glyc}	0.13	0.13
Lactonitrile formation	j_{lact}	0.04	0.04
Glycogen buildup	j_{stor}	0.71	0.71

Unfortunately, data on glycogen buildup is not available for *Saccharomyces cerevisiae.* Instead, we use data from experiments on glycolytic oscillations in *Saccharomyces carlsbergensis* [39]. Therefore, the estimates of metabolic fluxes are made by combining the data in refs. [5,39] (Table 8), so these estimates might not be very accurate for the situation considered.

3.3. Experimental limitations

The biochemical measurements of the Dutch group are of high quality. Still, there are inherent limitations to this kind of measurements, which are important to their use for model validation. Some metabolite concentrations are too low to be measured, and most others can only be measured with considerable error. This means that for most metabolites, oscillation amplitudes and phases are rather inaccurate, whereas average concentrations (used to estimate stationary concentrations) are more reliable. The biochemical measurements are made on samples taken from a suspension of oscillating yeast cells, so they might also have systematic errors arising from the difficulty of stopping all reactions immediately. (A special technique, where the reactions are stopped by spraying the sample into -40 °C cold methanol, was used to limit this problem [40].)

The CSTR set-up permits reproducible well-controlled experimental conditions for prolonged periods of time. This means that frequencies and relative amplitudes can be measured accurately and therefore, positions of bifurcation points can be determined precisely. For the same reason, perturbation experiments can be repeated under identical operating conditions, thereby ensuring accurate results.

So for each individual run, the CSTR measurements provide very accurate data. Unfortunately, there is inevitable variation between batches of cell suspensions used in the inflow (due to differences in cell density and exact harvesting time). Nevertheless, the data from these experiments are quite reproducible from run to run. Another problem with the CSTR experiments is that the measured fluorescence is proportional to the intracellular NADH concentration, but the proportionality constant is unknown. So we loose an absolute measure of the magnitude of the oscillations as discussed in Section 7.

The combined set of biochemical and dynamical experiments provides a large set of high quality data for model validation. It includes data related to properties of the system as a whole as well as data for specific metabolites, but all applying to the full system. Since our optimization scheme includes all of these data, we find it reasonable to embark on the optimization of a full-scale model of glycolysis.

4. Model

In this section, we establish the framework of metabolites, reactions, and rate expressions on which our glycolytic model is based. The stoichiometry of glycolysis (including the identity of the metabolites participating and the branchings/connectivity of the network) has been fully known for a long time, but some reactions can be lumped and some metabolites ignored in the modeling without sacrificing agreement with experiments. We explain how the need to compare with all available experiments (together with fundamental biochemical facts) dictates the metabolites and reactions to include (see Table 1 and Fig. 2), and describe how we have arrived at the rate expressions of the present model (Table 2).

The rate expression for a given reaction gives the velocity of the reaction as a function of the concentrations of metabolites and other species such as enzymes, activators, and inhibitors. This part of the kinetics of glycolysis is qualitatively well understood, and described (with the stoichi-

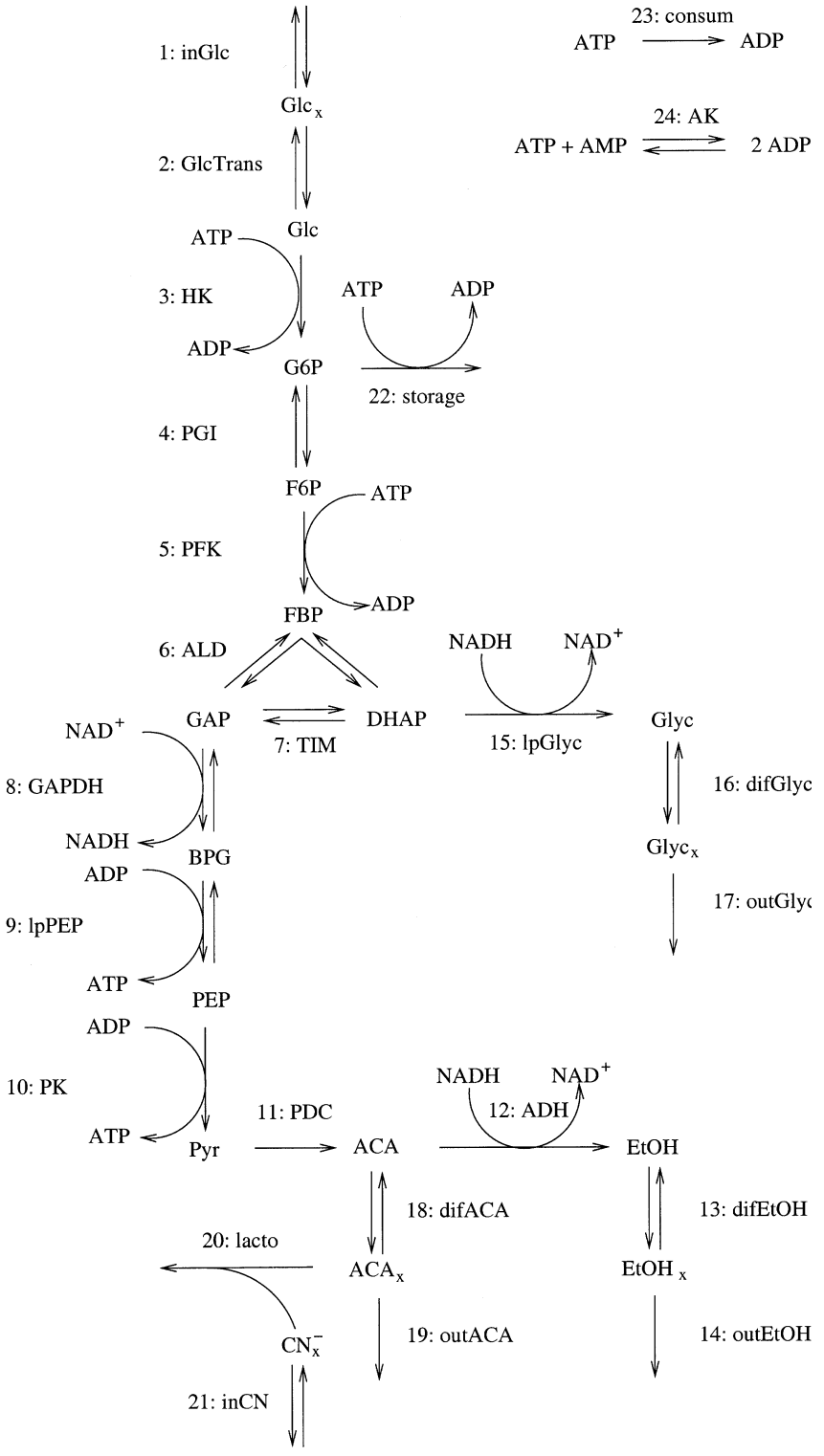

Fig. 2. Reaction network of the model.

ometry) in standard textbooks on biochemistry, although details of some of the rate expressions are less certain. In any case, it is the set of rate expressions that contains the considerable variability of the kinetics between different cell types.

A rate expression can often be expressed in a definite functional form containing kinetic parameters such as Michaelis constants in which the mathematical form is believed to be correct. Much of the variability and the least known aspects of glycolysis can be associated with the precise values of kinetic parameters for any given system.

Therefore, the strategy of our modeling is to work from a fairly complete, fixed 'skeleton' of rate equations building on the extensive biochemical knowledge of glycolysis, and use the experimental data described in the previous section to fit the set of unknown parameters. The precise choice of equations will, of course, influence the properties of the final model. We emphasize that the functional forms of the rate expressions have not been subject to optimization in this study although some details have been adjusted in the course of the project.

Recall that the experimental system is a stirred suspension of yeast cells in a CSTR. This means that there is a single homogeneous extracellular phase and many (in the order of one billion) intracellular cytoplasmic phases. Whether or not diffusion can keep each of these intracellular phases homogeneous is an open question, but we will nevertheless, assume that it can.

The yeast cells are known to synchronize their oscillations [6,18,19]. Based on the experiments discussed below, we assume that the synchronization is strong so that all the cells behave the same. Therefore, we model all the intracellular phases as one single phase, so the entire system is modeled as a two-phase system, as mentioned in Section 2. This assumption is not at all trivial; see refs. [41,42] for experimental studies and Matthews et al. [25] for a thorough theoretical and numerical investigation of coupled oscillators. However, for the particular experiments modeled here, there are several indications that the cellular oscillations are in fact essentially always synchronized, and that the emergence of oscillations at the observed bifurcation represents simultaneous Hopf bifurcations in each of the cells and not a gradual synchronization of already oscillating cells. Both the quenching experiments (which probe the geometry of dynamical structures in the concentration space) and the bifurcation analysis of the CSTR experiments show the behavior expected from a system close to a supercritical Hopf bifurcation.

This is illustrated in Fig. 1a,b and Fig. 7a as well as Fig. 10 (Appendix C). The rather sudden stagnation of the increase of amplitude seen in Fig. 7a is adequately explained as saturation of the glucose transporter (see Section 3), so this phenomenon is probably not caused by all oscillators reaching complete synchronization. The associated loss of sensitivity to glucose perturbations is a natural consequence of saturation, but cannot easily be explained in terms of synchronization. Furthermore, the mixing experiments [6,18,19] show that the synchronization is fast, which is another indication of strong synchronization. Finally, we note that in yeast extracts a bifurcation from a steady state to an oscillatory state is indeed found at low input rates of glucose or fructose when the input rate is increased [43] (whereas the bifurcation back to a steady state at high input rate in the same experiments is not found in the intact cells because of the saturation of the glucose transporter).

In the CSTR set-up, there are constant inflows of glucose solution, cyanide solution and cell suspension, and a constant outflow of reaction mixture. Therefore, all the metabolites in the model should in principle, be modeled with an inflow and outflow. However, flows of intracellular metabolites are not taken into account. Including these flows in the model would complicate the model significantly without gaining much in terms of biochemistry or realism. This is easily seen from a simple calculation; the intracellular glycolytic metabolite with the highest known concentration is pyruvate with a concentration of 8.7 mM. Since the specific flowrate of the CSTR is 0.048 min^{-1}, the outflow of pyruvate due to outflow of cells is 0.4 mM min^{-1}, which is negligible compared to the glycolytic flux of 27 mM intracellular glucose min^{-1}, estimated from the batch experiments of the Dutch group [5] (see page 111 of

Danø [30]). Therefore, we model the CSTR as if the cells were fixed in the reactor, while there is an inflow of glucose and cyanide solutions and an outflow of the extracellular reaction mixture. Apart from the immediate simplification of the model, this approximation also introduces two conservation equations, which simplify the optimization further (Table 1).

The experiments supplying the data for the optimization have set-ups that help minimize the size of the biochemical network, which we need to include in the model. The cyanide blocks the cytochrome *c* oxidase of the electron transport chain and consequently, pyruvate is not oxidized through the citric acid cycle; instead, it is fermented to ethanol. Since the yeast cells of the present work are starved beforehand and have no external nitrogen source available during the experiments, they will not be able to change their enzyme composition significantly during the experiments. Therefore, we model them as non-growing cells with a fixed enzyme composition, and we need only consider four branch points of the reaction network (see below for details on the explicit formulation of the model).

Since we want to include as large a set of experimental data as possible in the optimization, we need rate equations expressing all the experimentally measured properties. To this end, we expand existing glycolytic models of yeast extract. This approach results in a fairly large model, which includes processes associated with the membrane and the extracellular phase. In this way, we have focused on the application of the direct method of optimization and the incorporation of experimental data in the optimization, rather than the actual formulation of the model.

As a basis for our model, we choose the yeast extract model by Nielsen et al. [14] (which builds on previous work by Termonia and Ross [12], in particular) since this model describes the dynamics of cell extracts quite well: It predicts the same sequence of bifurcations and waveforms as is seen in a CSTR with yeast extract when the specific flow rate is varied, and it gives a reasonably good description of the response to perturbations. To obtain a model of intact yeast cells, some changes and extensions of this model are needed.

For obvious reasons, the membrane transport processes must be included. We have adopted the rate equation of the glucose transporter with G6P inhibition from Rizzi et al. [44] who obtained their rate expression by fitting kinetic parameters to Glc and G6P transients, caused by addition of a glucose pulse to a growing culture of glucose limited *Saccharomyces cerevisiae*.[3] The question of whether the glucose transporter is in fact inhibited by G6P is unsettled, but the optimization may select whichever choice makes the best fit, i.e. we tested it with and without inhibition. Since G6P appears as an inhibitor and is a branchpoint of the network eventually chosen, this metabolite must be explicitly included in our model. This is done by modeling the PGI reaction as in Richter et al. [11]. Three simple transport processes have to be included as well: diffusion of glycerol; acetaldehyde; and ethanol across the membrane with net flows from the cytosol to the extracellular medium.

Another feature that is important in a model of intact yeast cells is glycerol production. If an intermediate metabolite like acetaldehyde, which appears between the GAPDH reaction and the ADH reaction, is drained out of the pathway (e.g. by diffusing out of the cell), then the NADH produced in the GAPDH reaction would need to be reoxidized by some reaction other than the ADH reaction. This replacement is mainly achieved by the G3PDH reaction. We assume that dephosphorylation of glycerol 3-phosphate is fast, so we have lumped the G3PDH reaction and the glycerol phosphatase reaction into one reaction with the kinetics of the former as reported by Cai et al. [45]. This requires that DHAP appears explicitly in the model; we therefore, include the ALD reaction and the reaction catalyzed by TIM (both with rate equations from Richter et al. [11]). (See Table 8 for an estimate of the magnitude of the glycerol production.)

Some additional modifications have been made to the model by Nielsen et al. Since the ADH reaction is not near equilibrium, we prefer to model it as an irreversible reaction with Michaelis–

[3] Note that the lack of symmetry between the rate equations for the forward and reverse reactions is indeed correct; the equation for the reverse reaction is quoted incorrectly in Rizzi et al. [27].

Menten kinetics instead of a reversible bimolecular reaction [11]. This simplification is further justified by the experimental finding that the yeast cells are insensitive to EtOH perturbations [4].

Similarly, we prefer to model the GAPDH reaction as a reversible reaction because it is close to equilibrium. For this purpose, we have adopted the rate equation from Teusink et al. [1]. Also, a negligible term of the denominator of the PFK rate expression has been left out.

Initially, the reactions catalyzed by HK, PK and ADH were modeled as ordered BI BI reactions [46] reduced to an irreversible form. In the course of the optimization, it turned out that the rate equations for the PK and ADH reactions could be simplified to the forms given in Table 2, whereas the HK reaction could not be simplified in this way.

As discussed in the previous section, the glycogen production is substantial in experiments with starved yeast cells, so we include it in the model as well. (The UTP required for this reaction is counted simply as ATP.) Experiments have shown that the lactonitrile-forming reaction between acetaldehyde and cyanide is important for the dynamics of synchronized glycolytic oscillations [5,19]. Therefore, this reaction is also included. Since we model glycolysis in a stationary state, it is necessary to include processes consuming ATP (and producing ADP). We model such processes schematically with a simple first order reaction. We may think of this ATP hydrolysis as driving some basic cellular demands like the maintenance of membrane potentials. Finally, the inflows and outflows of the CSTR are modeled for extracellular species as discussed above, and the F6P drain is removed since we are modeling non-growing cells.

The above changes and additions to the model by Nielsen et al. [14] result in the model presented in Table 2 and sketched in Fig. 2. For the form of the rate equations and the significance of the parameters, we refer to the papers referenced in Table 2. A discussion of these questions is outside the scope of this paper.

With this huge model, we can capture most of the available experimental observations of our specific system. An obvious drawback is that the model now has a large number of parameters. Furthermore, the dynamics of the unoptimized model does not fit the experimental observations *at all*. However, since most of the equations are taken from other models or directly from enzyme kinetic studies, we have some reasonable parameter values for the start of the optimization and, as we shall see, most of the kinetic parameters can retain their literature values.

5. Calculation

Reaction velocities depend on a number of kinetic parameters (velocity parameters and intrinsic parameters) as well as on substrate concentrations, as in Table 2. For a given set of intrinsic parameters, a unique stationary state is completely determined by a set of stationary reaction velocities together with a set of stationary substrate concentrations. From these sets, one can calculate the velocity parameters and all local dynamical properties through algebraic calculations.

The optimization of the model can now be succinctly described as follows. We first fix all the known intrinsic parameters and stationary concentrations to their experimental values. Next we generate 'all possible' sets of stationary reaction velocities (as described in Section 5.1 and Appendix B), together with all sets of unknown concentrations and unknown intrinsic parameters (within bounds that may be inferred from experiments). For each set, we calculate the model prediction of experimentally known dynamical properties (as shown in Section 5.2) and compare them with the experimental values. The search is described in Section 5.3. The set for which the predicted properties best agree with the experiments is used to calculate the set of velocity parameters as described in Section 2.2. Together with the intrinsic parameters, this set determines the best possible model for the reaction system. The relevant stationary state of that model is given by the set of concentrations used as 'input'.

5.1. Specification of a model at a stationary point

An instantaneous reaction velocity of the reaction system is a vector **v** with the velocities of all the reactions as components. For the model of

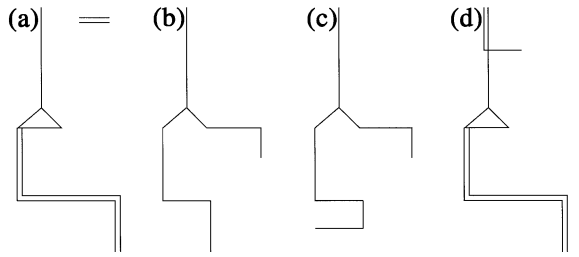

Fig. 3. Schematic representation of the four irreducible subnetworks patterned on Fig. 2. (a) Glycolysis and fermentation, $\mathbf{E}_{ferm}$; (b) glycerol production, $\mathbf{E}_{glyc}$; (c) glycerol production and lactonitrile formation, $\mathbf{E}_{lact}$; and (d) glycolysis, fermentation and glycogen formation, $\mathbf{E}_{stor}$.

glycolysis given in Table 1, there are 36 components of which 12 are reverse reactions of reversible pairs. Thus, the velocity space has 36 dimensions. The space of *stationary* reaction velocities has much lower dimension (16 as we show below), and the efficient handling of these are at the heart of the direct method of optimizing models. The method uses a straightforward mathematical procedure, outlined in Appendix B. Here we present a biochemical argument for the representation of stationary reaction velocities for the model of glycolysis.

We first look at stationary *net velocities*, i.e. for reversible reactions the differences between forward and reverse velocities. We note that the 'network' of reactions shown in Fig. 2 has chains of reactions branching like a tree. This structure makes it easy to determine all possible stationary net velocities. These are linear combinations with non-negative coefficients of suitably normalized net velocities for each of just four definite subpathways, which cannot themselves be expressed similarly in terms of linear combinations of simpler subpathways. They are shown in Fig. 3. We might call such subpathways 'irreducible'. The stationary velocities of such networks have been called 'extreme currents' [47]. 'current' is short for 'stationary reaction velocity', whereas the term 'extreme' can be understood from a geometrical interpretation given in Appendix B.

Each subpathway must start with extracellular glucose entering the system and end with one or more extracellular species leaving the system or with accumulation of glycogen. (We do not require stationarity for glycogen.) The possible branchings are limited by the stationarity condition for the conserved pair, NADH and NAD^+. So if a subpathway contains reactions producing NADH, it must also contain other reactions consuming the same number of molecules NADH. The same applies to ATP and ADP, when we take into consideration other reactions in the cell external to glycolysis producing ADP from ATP. These reactions are represented by the schematic reaction R23 in the model (and see the discussion of glycogen formation below). Consequently, from the point of view of glycolysis proper, there is the restriction on stationary (sub-) networks that although ATP may be produced, it must not be consumed, and *vice versa* for ADP. For glycolysis plus reaction R23, ATP and ADP together are conserved at stationarity. We include the adenylate kinase reaction, R24, between ATP and AMP for the sake of dynamics. It has net velocity zero at stationarity, so AMP can be ignored as far as stationarity is concerned.

Glycolysis followed by fermentation and outflow of extracellular ethanol, can be stationary together with R23, and cannot be expressed as a combination of simpler stationary networks (see Fig. 3a). The NADH formed in the GAPDH reaction is reoxidized in the ADH reaction. Two molecules of ATP is formed (per molecule Glc), which are used elsewhere in the cell, reaction R23.

If acetaldehyde escapes the cell, it is lost for the last step of fermentation, the reduction to ethanol, and the NADH produced in the GAPDH reaction must be reoxidized elsewhere. Consequently, glycerol must be produced and flow out. So the GAP and DHAP formed together in the ALD reaction proceed along different branches; while GAP is oxidized by NAD^+, DHAP is reduced by NADH, and there is no net production of either NAD^+ or NADH. The extracellular acetaldehyde formed in the branched process just described, can either flow out or react with cyanide to lactonitrile, giving rise to two distinct irreducible subpathways (Fig. 3b,c). The two molecules of ATP hydrolyzed in the upper part of glycolysis are reproduced in the branch from GAP in the lower part.

Finally, we consider glycogen formation via G6P. This reaction cannot occur alone at stationarity because ATP is consumed. The only way this can be compensated is if one molecule glucose is degraded through glycolysis and fermentation (all the way to extracellular ethanol flowing out) for each molecule of glucose that is build into glycogen (see Fig. 3d). Note that although this subpathway in a sense, contains glycolysis with fermentation as a part, it cannot be expressed in simpler terms because the two parts always must take place together in order to maintain stationarity, when glycogen is formed.

Now we may choose a stationary net velocity vector for each of the four irreducible subpathways (a matter of scaling or 'normalization'), $\mathbf{E}_{\mathrm{ferm}}$, $\mathbf{E}_{\mathrm{glyc}}$, $\mathbf{E}_{\mathrm{lact}}$ and $\mathbf{E}_{\mathrm{stor}}$. Then, any stationary net velocity, $\mathbf{w}$, can be expressed as a linear combination with non-negative coefficients of these four 'extreme' net velocities,

$$\mathbf{w}=j_{\mathrm{ferm}}\mathbf{E}_{\mathrm{ferm}}+j_{\mathrm{glyc}}\mathbf{E}_{\mathrm{glyc}}+j_{\mathrm{lact}}\mathbf{E}_{\mathrm{lact}}+j_{\mathrm{stor}}\mathbf{E}_{\mathrm{stor}}, \qquad (5)$$

a 'convex combination'. (The indices refer to the irreducible subpathways representing fermentation, glycerol production with outflow of ACA, glycerol production with lactonitrile formation, and storage buildup, respectively.) A set of four non-negative coefficients (which we refer to as convex coefficients) uniquely determines the net velocity for our particular model (but see the brief discussion of redundancy in the general case in Appendix B).

With the definition of reaction velocities given in Section 2, we can now exhibit in Table 3 the four 'extreme currents' with the normalizations chosen (explained below). The components shown are integers, which are directly related to the stoichiometry of the reaction chains. As velocities they are measured in a common unit, v_0, which we choose to be the rate of flow of glucose into the cells (apart from that built into glycogen), as estimated from the production of ethanol and glycerol in the batch experiments [5], approximately 27 mM/min (expressed as an intracellular velocity).

The precise normalizations are not really important to the optimization, but a rational choice may help us understand the significance of any particular set of convex coefficients. The normalization used in Table 3 is such that each of the extreme currents alone would consume glucose with a rate, v_0 (disregarding the part stored in glycogen). It is sometimes convenient to define

$$j_0=j_{\mathrm{ferm}}+j_{\mathrm{glyc}}+j_{\mathrm{lact}}+j_{\mathrm{stor}} \qquad (6)$$

and to refer to a linear combination of (normalized) extreme currents with non-negative convex coefficients satisfying $j_0=1$ as a normalized net velocity.

It is possible to treat all reactions (forward or reverse) on an equal footing. Then one gets one additional extreme velocity for each pair of reversible reactions. However, these are so simple that reversible reactions can be better handled more informally. For each reversible reaction, we can get a pair of separate forward and reverse velocities from the net velocity by choosing any non-negative velocity for the reverse reaction and add it to the stationary net velocity to get the forward velocity. This can be done independently for each reversible pair. Since there are 12 pairs of reversible reactions in our model of glycolysis and the space of stationary net velocities is four-dimensional, the space of stationary velocities has 16 dimensions.

In summary, to uniquely specify any possible stationary reaction velocity for the model of glycolysis, we must supply a set of four non-negative (unnormalized) convex coefficients and a set of 12 velocities for the reverse reactions. These 16 values together with the 20 stationary concentrations (36 values, altogether) then determine the system of 36 reactions and a stationary state for that system, when combined with all the intrinsic parameters. In practice, constraints imposed by the experimental set-up may reduce the number of independent variables, as will be discussed in Section 5.3.

5.2. Properties of a model at a stationary point

The direct method of fitting a model can be used whether or not dynamical properties of the system are known, provided enough other data are available. Here we first discuss the dynamical properties that are experimentally available for glycolysis. Then we explain how such properties

are calculated for a model in the course of an optimization.

Quite a large set of dynamical data are available for glycolysis from the CSTR experiments [4] and from the Dutch batch experiments [6,7]. From the transient oscillations of the batch experiments, we can get an estimate of the phases for the oscillations of the concentrations of several species relative to that of NADH. We can also get rough estimates of relative amplitudes. These data have been included as explained in Section 5.3.

Recall that the CSTR experiments were made at oscillatory states, not at a stationary state. However, the oscillatory states were so close in parameter space to a Hopf bifurcation (where a stable stationary point becomes unstable and sustained oscillations appear spontaneously) that the properties at the bifurcating stationary state can be inferred by extrapolation or by approximation. We fit the model to experimental data at a stationary point at a Hopf bifurcation point.

From the CSTR experiment, we get an accurate determination of the frequency of oscillation at the bifurcation, ω_0, by extrapolation. This is the imaginary part of the eigenvalue λ, associated with the oscillation, $\omega_0 = \mathrm{Im}\{\lambda\}$. The real part of λ vanishes at the Hopf bifurcation, $\mathrm{Re}\{\lambda\} = 0$, so if we consider only Hopf bifurcation points, we automatically fit $\mathrm{Re}\{\lambda\}$ to its experimental value as well.

In addition to these two real parameters, the CSTR experiments provided four other real values, namely two quenching concentrations and two associated quenching phases relative to the phase of [NADH]. In practice, we can only utilize the ratio of the two quenching concentrations (because we cannot relate them to the amplitude of the oscillations, which are monitored as the fluorescence). So the CSTR experiments provide data on five dynamical variables.

In the present section, we show how one can calculate these experimentally accessible variables from a model in a stationary state so that they can be utilized for optimizing the model. They can be calculated for a model when we know all the parameters of the model and all the concentrations at a stationary point. However, we shall calculate the dynamical data from a different set, namely from the intrinsic parameters together with the *stationary reaction velocities* and the stationary substrate concentrations. The dynamical properties discussed here are special cases of general local dynamical properties that may become accessible experimentally (see Section 9) and calculated from a model, whether or not the system is oscillatory or at a bifurcation.

The kinetic equations were expressed in terms of the reaction velocities as Eq. (2) in Section 2. For a given model, the velocity v_r of a reaction r is a function of the set of concentrations **c**, and with that dependence made explicit, Eq. (2) can be written in vector notation as

$$\dot{\mathbf{c}} = \mathbf{f}(\mathbf{c}). \tag{7}$$

At stationarity, $\dot{c}_s = 0$ for each species s, so Eq. (2) shows that the stoichiometric matrix maps any stationary velocity vector into a zero vector; a stationary velocity vector lies in the null space of the stoichiometric matrix. This observation is important to the particular representation of stationary states used here, as discussed in Appendix B.

Close to stationarity, the motion in concentration space can be approximately described by linearized kinetics, Eq. (4), in terms of the Jacobi matrix **J** at the stationary state. Thus, the local dynamical properties of the reaction system are (largely) determined by **J**. By definition, **J** is the derivative of the field **f** with respect to **c**, and usually the result is expressed explicitly in terms of **c**. However, for our purposes, it is convenient to retain an explicit dependence on **v**:

$$y_s J_{sp} = \sum_r \nu_{sr} \frac{\partial v_r}{\partial c_p} = \sum_r \nu_{sr} v_r \frac{\partial \ln v_r}{\partial c_p}. \tag{8}$$

so that the explicit dependence on **c** comes through $\partial \ln v_r / \partial c_p$ only (parametrized by the intrinsic parameters). The second form of Eq. (8) has no explicit dependence on rate constants or maximum velocities because these disappear as a result of the logarithmic derivation. This means that the local dynamical properties of the system can be calculated without knowledge of the velocity parameters, which is fortunate since these depend on the enzyme activity inside the cells (which are difficult to assess). This feature is essential to the

method being described. The numerical evaluation of the Jacobi matrix [Eq. (8)] is straightforward for any given sets of stationary velocities **v** and stationary concentrations **c** as the sum of products given by Eq. (8).

The local dynamical properties of the system can be best characterized through the eigenvalues and eigenvectors of the Jacobi matrix, **J**. Some of these can be determined experimentally as indicated in Section 2 (and see also Mihaliuk et al. [48]). For glycolysis, we have data associated with the oscillatory mode, so we need a pair of complex conjugate eigenvalues together with the associated right and left eigenvectors. They are calculated as described in Section 6.

The real part of the eigenvalue for the oscillatory mode is used to find a Hopf bifurcation as described in Section 6, and the imaginary part gives the frequency of oscillation there. For a bifurcating stationary point, one can then determine the amplitudes and phases of the oscillations of each species from the right eigenvector and the quenching concentrations and quenching phases for each species from the left eigenvector corresponding to the oscillation as indicated in Section 2.

Other linear dynamical properties can be calculated from other eigenvalues and eigenvectors, and non-linear properties can be obtained through higher order derivatives of the vector field **f** of Eq. (7). These non-linear properties require a great deal more calculation, and we have only used these for the final model resulting from the optimization, not during the optimization (see Section 6 and Appendix C).

5.3. Search for best fit

To fit a model to experimental data, we first assign all the known 'free' variables to their experimental values. Then, we step through all possible sets of unknown free variables in intervals estimated to be relevant, with a reasonable resolution (stepsize) for each variable. The free variables that can be assigned or scanned comprise intrinsic parameters, convex coefficients, reverse reaction velocities (or reverse/forward velocity ratios), and stationary substrate concentrations.

From the convex coefficients, we calculate the set of stationary net velocities. These combine with reverse/forward velocity ratios to yield separate forward and reverse velocities for reversible reactions. Once all free variables have been assigned, we calculate some or all relevant dynamical properties of the system. In general, these can be compared with experiments at this stage. In the present study, the experimental data apply to a Hopf bifurcation, so we need only calculate an eigenvalue, λ, associated with the oscillations. When we observe a change of sign of the real part of that eigenvalue, $\mathrm{Re}\{\lambda\}$, we use a root searching algorithm to find a zero of $\mathrm{Re}\{\lambda\}$, as described in Section 6. Only when we have found such zero, do we calculate all of the relevant dynamical properties and compare with experiments.

Recal from Section 2 that a point is a set of variables and parameters that is necessary and sufficient to define a system and a stationary state of that system. So in principle, we systematically scan all points in all relevant regions of unknown variables and parameters with some finite resolution and, for each point, we calculate the properties of the system and compare with experiments. During the scan, the velocity parameters are unknown, and there is no need to calculate them (although the calculation is very simple and can be done if desired). Only at the end of the optimization, the velocity parameters (rate constants and maximum velocities) are calculated for the point (or small set of points) providing the best possible agreement with experiments.

The general procedure outlined above usually needs modification due to system specific conditions. In the remaining part of this section, we shall describe the modifications applying to the special system treated here, a suspension of yeast cells in a flow reactor, and make comments relevant to that system.

Although, broadly speaking, the immediate goal of the optimization is to determine the velocity parameters, some of these are actually interrelated or known and related to free variables. For the passive transport of Glyc, ACA and EtOH, the ratio of the rate constants are known (estimated from empirical formulas for fat/water partitioning ratios [49]), so here, only one of them is scanned.

The rate constants for the inflow and outflow reactions for the extracellular species are all given by the specific flowrate k_0, which is a purely mechanical parameter that is controlled and known. When a velocity parameter is known, the associated rate expression is used to calculate a concentration instead, whether or not it is known experimentally, as we discuss below. Thus, such concentration is not free, and we cannot consistently assign it an experimental value. Instead, we must compare its calculated value with experiment on a par with the comparisons of dynamical properties.

In glycolysis, many intrinsic parameters are known. All the unknown intrinsic parameters must be scanned. Stationary net reaction velocities are always calculated from the extreme currents. For glycolysis we have estimates of the convex coefficients (from production rates of ethanol and glycerol in batch experiments [5]), but the estimates are not very accurate, so we scan fairly narrow intervals of these parameters.

In scanning over all stationary net velocities, it is convenient to first scan over all relevant normalized velocities (see Section 5.1) and subsequently, scan over all relevant magnitudes of the velocity. A normalized velocity determines the fractions of the glycolytic flow that go through the different branches. The magnitude of the velocity vector, $j_0 v_0$ determines in a rough sense, the total glycolytic flux, namely the rate of consumption of glucose disregarding the part that goes to glycogen build up. That magnitude is a prime factor determining the frequency of oscillations near a Hopf bifurcation (see the section 'A scaling principle' in Hynne et al. [2]). It also determines the extracellular glucose concentrations $[\mathrm{Glc}_x]$ (which is also known experimentally), and maintaining agreement with frequency and $[\mathrm{Glc}_x]$ simultaneously constitutes an important restraint during the optimization.

For each pair of reversible reactions, we must determine the separate forward and reverse reaction velocities from the net velocity. For all but one of the 12 pairs of reversible reactions, the forward or reverse velocity or the reverse/forward velocity ratios are known or can be calculated from the stationary substrate concentrations (in terms of known rate constants or equilibrium constants).

So for each of these, the separate forward and reverse reaction velocities can be calculated from the net velocities. The method for this has already been indicated above for the reversible inflow/outflow reactions and for the passive membrane transport reactions. Note in R6 that the velocity parameter V_{6f} appears in the denominator only as the ratio V_{6f}/V_{6r}, which can be scanned. The AK reaction, R24, is at equilibrium in the stationary state since it has zero net velocity (to get stationarity with respect to AMP). So the forward and reverse velocities are equal and may be scanned.

The only reaction for which the reverse/forward velocity ratio needs to be scanned is the lumped PGK, PGM and ENO reactions, R9. For this reaction, the velocity ratio is scanned over a suitable interval and, for each value, the separate velocities are calculated using the net velocity.

Most stationary concentrations are known for glycolysis (estimated from batch experiments [7]), and there are dependencies between some concentrations and velocities. All extracellular concentrations are connected with net inflow or outflow velocities through the specific flowrate k_0 and mixed flow concentrations. For example, the mixed flow concentration of extracellular glucose determines the velocity of the flow of glucose into the reactor, and together with the net inflow velocity this gives the velocity of the outflow of extracellular glucose and hence, its concentration $[\mathrm{Glc}_x]$. The same applies to cyanide.

Similarly, the extracellular concentration of glycerol can be calculated from the velocity of the flow of glycerol out of the reactor, and from that concentration, the velocity of the membrane transport of glycerol into the cells can be calculated from the current value of the rate constant, which is scanned. And that velocity together with the net membrane transport velocity in turn, determines the velocity of the transport of glycerol out of the cell, which further determines the intracellular concentration of glycerol. The same procedure can be used to calculate similar quantities for acetaldehyde and ethanol using the estimated ratios of rate constants mentioned above.

6. Implementation

The work of optimizing a model has several stages. First, we find the extreme currents for the given mechanism. (Only the stoichiometry needs to be determined at this stage.) When the pathway is sufficiently simple, this can be done by inspection as we did in Section 5.1. If the number of extreme currents exceeds the net number of reactions minus the number of species, we must find a 'partition of the current polytope into simplices' as described in Appendix B. Fortunately, this step in not necessary for the model of glycolysis studied here. (By net number of reactions, we mean the number of forward reactions minus the number of reverse reactions — in other words, the number of reactions counting each reversible pair as one.)

The next stage in the overall procedure is to create a program for the optimization. The structure is indicated below.

The third stage is the optimization proper in which we scan part of the space of unknown parameters and variables. The convex coefficients are scanned with selected step intervals. For all other parameters and variables, the possible values sometimes span several decades, so these are scanned with selected step factors. In the present work, the first task is to find regions (of the set of unknown variables and parameters) where the system shows oscillations, i.e. where the spectrum of eigenvalues of the Jacobi matrix includes a complex conjugate pair. The next thing to worry about is the stability of modes. We need regions where one oscillatory mode can become unstable whereas all other modes are stable. In these initial searches, it is sufficient to determine the set of eigenvalues of each point, which is much faster than finding also the eigenvectors.

In the final phase of the optimization proper, we search relevant regions found in the initial phase, locate Hopf bifurcations, calculate the relevant dynamical properties of the model at the bifurcations, and compare these with the experimental values. A Hopf bifurcation is located as a point where the real part of the eigenvalue of the (relevant) oscillatory mode becomes zero using a root-finding algorithm. Eigenvectors need only be calculated at the end when a zero has been found and the frequency of oscillation meets given criteria.

When the best possible fit of model properties to experimental values has been found, the resulting rate constants and maximum velocities are obtained from Eq. (3) and all data of the optimum model are collected. In practice, we do not obtain one perfect fit, but must choose the 'best' one through a somewhat subjective compromise between conflicting criteria. Therefore, we record data for all points meeting less strict criteria and select a best fit by searching and filtering the output.

At this stage, the best model has been found, but we still need to make sure that the bifurcation is indeed a supercritical Hopf bifurcation. It could just as well be subcritical and, in this case, the model would not be entirely acceptable, suggesting continued search. The most straightforward way to determine the character of the bifurcation is to calculate the normal form parameters. We explain the meaning of the normal form and exhibit the parameters of the normal form equation and of a transformation from normal form coordinates to real chemical variables in Appendix C.

Actually, we calculated one of the normal form parameters, σ' (see Table 9 and Appendix C), during the optimization with a special method building on an interpretation of the normal form. The sign of this parameter determines the 'direction' of the bifurcation and it was necessary to check it because it was wrong in a large fraction of the bifurcation points found. (Experimentally, the sign is positive meaning that the oscillations emerge for increasing values of the mixed flow glucose concentration.) The other normal form parameters were not calculated until a potential 'best point' was found because the computation of these parameters is much too time consuming.

As a check, we also integrate the kinetic equations of the model with all the parameters as determined at the optimum, and using the optimum concentrations as initial values. Since, by design, the concentrations correspond to a stationary state, all concentrations must remain absolutely constant in the integration provided the values for all parameters and initial concentrations are given with high accuracy. This check on the consistency

Table 9
Comparison with experiments: dynamics [see also Fig. 10 and the definitions of parameters in Appendix C (experimental data from Danø et al. [4] as described in text)]

	Parameter	Model	Exp
Angular frequency at bifurcation	ω_0 (min^{-1})	0.05	10.05
Rate of change of instability[a]	σ' (min^{-1})	0.0579	>0
Rate of change of frequency[a]	σ'' (min^{-1})	−0.112	
Non-linearity parameter, real part	g' (min^{-1})	−1124	<0
Non-linearity parameter, imaginary part	g'' (min^{-1})	−1586	>0
Rate of change of amplitude[b]	$2\sqrt{-\sigma'/g'}$	0.0144	
Rate of change of frequency[c]	$(\sigma''-\sigma' g''/g')$ (min^{-1})	−0.194	0.055

[a] At the stationary point as a function of μ.
[b] Of the limit cycle as a function of $\sqrt{\mu}$ in units of mM NADH.
[c] Of the limit cycle as a function of μ.

of data set and model is extremely sensitive to errors. To enable users of our data to make such check, we give the model parameters with much higher precision in the tables of Section 7 than would otherwise be appropriate. We also integrate the kinetic equations to investigate the behavior of the model in the neighborhood of the bifurcation point, determine bifurcation diagrams, study synchronization behavior, etc. as reported in Section 8.

We briefly indicate the structure of the program and give some details of the algorithms. After initialization, partly from an input file specifying the run mode, where to search, and criteria for output, etc., the main part consists of nested loops for scanning intrinsic parameters, convex coefficients, reverse reactions, and concentrations.

The inner loop basically treats one 'point'. It calculates net velocities from convex coefficients, then all velocities using also information about reverse velocities. At this stage, variables are adjusted for interdependencies, which would be awkward to account for in the loop structure. Now the Jacobi matrix is calculated using Eq. (8) and diagonalized. If only eigenvalues are needed, we use a QR algorithm for a matrix obtained from **J** by balancing and reduction to Hessenberg form as described in Press et al. [50]. When the eigenvectors are needed as well, we use the algorithm by Eberlein (see Wilkinson and Reinsch [51]).

In the early phases of an optimization where we look for regions of stationary states with stable or unstable oscillatory modes, we simply output one character summarizing the properties of the stationary state, and go on to the next loop iteration. In the later phases when we search for Hopf bifurcations, we test whether there is an oscillatory mode, if the previous point had an oscillatory mode as well, and if there is a change of sign of the real part of the eigenvalue, λ, associated with that mode between the previous point and the present one. (The inner loop variable is carefully selected to suit the search for Hopf bifurcations; in the present optimization, we search with the intracellular glucose concentration.)

If all tests indicate that a Hopf bifurcation might be found for some value of the inner loop variable in the interval between the last two points, we enter a search for the bifurcation point using an algorithm due to van Wijngaarden, Dekker and Brent (see Press et al. [50]). The algorithm finds a zero of $\mathrm{Re}\{\lambda\}$ and the frequency of oscillation at that point as $\omega_0 = \mathrm{Im}\{\lambda\}$. If the frequency agrees with the experimental value to within assigned limits, the eigenvectors associated with the oscillatory mode are calculated and, from these, the desired dynamical properties of the model are found, in particular, amplitudes and phases of oscillatory concentrations, and quenching concentrations and quenching phases of species.

The calculated dynamical properties are compared with experimental values, and if all properties agree to within assigned limits, all or selected parts of the data for the bifurcating stationary point are output. In any case, the calculation proceeds to the next loop iteration.

We may give an indication of the capabilities and limitations of the method. For the rather large model studied here, we can look for oscillations and stability at a rate of approximately 5000 points/min on a HP 715/75 workstation. When we find the Hopf bifurcation, calculate the eigenvectors and velocity parameters, and print the results, the rate is much lower, depending very much on how often eigenvectors must be calculated. In our final scans with a large fraction of Hopf points, we could treat well over 400 points/min. This means that we can easily investigate millions, but not billions of points. In any case, it is impossible to really search *all possible* combinations of unknown free variables with any reasonable resolution. That conclusion remains true even for a much faster computer run in a much longer (realistic) period of time. The problem is simply too big. Even so, we have obtained points with good agreement for many variables, a result that would be hard to obtain with fitting using integration of models.

7. Results

The optimization is based on local properties of the system (i.e. properties in an arbitrarily small neighborhood of a point in concentration space). The local results can be expressed in tables, which we present in this section. The resulting model will be evaluated outside the particular point of optimization in the next section through integration of the kinetic equations and with continuation methods. We also briefly comment on the question of synchronization of oscillations in different cells there. More complex (higher order) local properties are discussed in Appendix C.

The result of the optimization consists first of all of the *maximum velocities and rate constants* calculated from the chosen optimum point. These are exhibited in Table 4. Equally important are the conditions for which the optimum occurs and the agreement of properties of the selected model with experiment. The rate constants and maximum velocities of the enzymes are difficult to measure, and we have no means to compare the results of Table 4 with experiments.

The model as such is defined by the maximum velocities and rate constants of Table 4 together with the *intrinsic parameters* (mainly Michaelis constants), which are selected as part of the optimization process. These are shown in Table 5 together with the literature values. As can be seen from Table 5, the intrinsic parameters are generally in good agreement with the biochemical literature. For some parameters, we were unable to find any relevant biochemical data. In these cases, we have listed parameters used in other glycolytic models in parentheses. (The rate constants k_{13}, k_{16} and k_{18} in Table 5 are repeated from Table 4 to exhibit their interrelation used in the optimization.)

The only major discrepancies between experimentally determined intrinsic parameters and those of the model are the values of K_{3Glc} and K_{4eq}. These parameters could not come closer to the experimentally reported values without seriously impairing the overall fit of the model. The constant K_{15DHAP} may appear to disagree with the experimental value, but this is due to the fact that K_{15DHAP} in the model includes the effect of inorganic phosphate (11 mM; Richard et al. [7]) found in the yeast cells (see Cai et al. [45] for details on the effect of P_i on G3PDH). The equilibrium constant K_{7eq} is also somewhat off. This is due to an internal inconsistency of the experimental data, which is discussed below in connection with the result for the stationary metabolite concentrations.

To completely define the model, the kinetic parameters must be *supplemented* with the value of the ratio between the extracellular volume and the total cytosolic volume, y_{vol}, given in Table 7. It can be considered part of the specification of the operating point insofar as it depends on the cell density of the suspension, but it may be said to enter the kinetic equations of the two-phase model in a more fundamental way than other operating point data [see Eq. (2) in Section 2.1]. As we mentioned in Section 3, we could not determine a consistent value for y_{vol} from data in the literature, but for an order of magnitude comparison, we quote a value deduced from comparable batch experiments [7] in Table 7.

It is particularly important to evaluate the model for the specific conditions used for the optimization. These are specified by the *operating point*

shown in Table 7. Besides the volume ratio y_{vol} expressing the cell density of the suspension, this is given by the flow rates of the CSTR at the bifurcation point; the specific flow rate and the mixed flow concentrations of extracellular glucose and cyanide. These flow rates agree exactly with the conditions of the experiment, i.e. it is possible for the model to work at the experimental operating point. (Table 7 also shows two fluxes characteristic of the metabolitic activity. These are discussed below.)

Once the operating point has been specified, we have a self-contained model for which the properties can be investigated by integration. However, we know beforehand that if the operating point is chosen as in Table 7, the model has a stationary state with *stationary concentrations* given by Table 6, and indeed that a supercritical Hopf bifurcation occurs exactly at that point (with the mixed flow glucose concentration as bifurcation parameter). These properties were used to select the best point in the optimization process. Note, however, that the stationary point shown in Table 6 need not be unique; there could be other (stable or unstable) stationary states for the same model and operating point, and other persistent states like, e.g. stable limit cycles could also co-exist with the stationary point of Table 6.

These remarks on possible non-uniqueness are really irrelevant to the optimization insofar as we have no knowledge of such behavior either in the model or in the experiments. We only mention the possibility to emphasize that once the model has been obtained, it remains well defined even without knowledge about the point in concentration space shown in Table 6. That said, the fact that we have a bifurcating stationary point that is designed to model a specific bifurcating stationary point in a well-defined experiment is very important. It is a rich source of additional experimental data that can be immediately compared with the model. Table 6 makes that comparison as well.

By design, the stationary concentrations predicted by the model agree very well with experiments. The concentrations of G6P, F6P, FBP, GAP, PEP, Pyr, ATP, ADP, AMP, NADH and NAD^+ agree with the batch experiments within experimental error, assuming that these intracellular concentrations do not change much from the bifurcation point used to the conditions of the batch experiments; DHAP is 18% higher than the reported value. However, this is due to an inconsistency in the experimental data: with the experimental values of [GAP] and [DHAP], and the experimental equilibrium constant K_{7eq}, the TIM reaction is almost at equilibrium; in fact, it has a small net velocity in the direction from GAP to DHAP, i.e. opposite to the substantial net flux (≈ 23 mM min^{-1}) from DHAP to GAP required by other reliable experimental data. Therefore, [DHAP] has been increased a little in order to obtain a reasonable value for the equilibrium constant K_{7eq} of this reaction, somewhat higher than the experimental value (see Table 5).

As explained in Section 3, the extracellular species measured in batch experiments ($EtOH_x$, ACA_x and $Glyc_x$) are not directly comparable to those at the Hopf bifurcation in the CSTR. The extracellular glucose concentration has been measured in the CSTR (this study), and the model agrees with this value within 5%.

A property of the model of considerable biochemical importance is the *total glycolytic flux* (defined, e.g. as the velocity of the PFK reaction) and the contributions to that flux from the various branches: fermentation; glycerol formation (with or without lactonitrile formation); and glycogen buildup. Table 7 shows the total glycolytic flux. It agrees with estimates from comparable batch experiments as discussed in Section 3. A related measure of overall metabolic rate is the cellular glucose uptake activity, also shown in Table 7, which includes the glucose build into glycogen. By our convention, it is given as an intracellular velocity (and equals, e.g. the velocity of the HK reaction because of stationarity).

Table 8 shows the *branching fractions* of the glycolytic flux together with values deduced from experiments as discussed in Section 3. We see that the model branchings agree with the experimental estimates. As an illumination of the meaning of these figures, we note that the storage process contributes $j_{stor}\, j_0 v_0$ to the glycolytic flux and the same to glycogen build-up, so the total glucose uptake rate can also be calculated as $(1+j_{stor})j_0 v_0$,

which agrees with the figures quoted in Table 7 (to within rounding errors).

Comparison of *dynamical properties* of the model with experiments forms a significant part of the optimization, and Tables 6 and 9 show how close an agreement was possible to attain. First of all the model has a Hopf bifurcation at the experimental value of the mixed flow glucose concentration (a pair of complex conjugate eigenvalues become pure imaginary, see Table 10 in Appendix C). The bifurcation is supercritical (g' is negative) and occurs in the correct 'direction' (σ' is positive), so the limit cycle oscillations appear for increasing values of the mixed flow glucose concentration; these features agree with the experiments.

The angular frequency ω_0 of the model (which is $2\pi/T_0$ with T_0 the period of oscillations near the stationary point at the bifurcation), is in perfect agreement with the CSTR experiments as Table 9 shows. Of the other quantities in Table 9, we have only data for comparison for the rate of change of frequency of the limit cycle oscillations with the mixed flow glucose concentration. It has a wrong sign in the model, which predicts that the frequency decreases with the mixed flow concentration, whereas in fact it increases.

Other dynamical properties that have played an important role in the optimization are compared with experiments in Table 6. These include, first of all, the fairly accurate quenching data obtained from the CSTR experiments. We see from Table 6 that the quenching phases ϕ_s for extracellular glucose, Glc_x, and for extracellular acetaldehyde, ACA_x, agree to within 9° of the experimental values. The experimental quenching concentrations q_s must be scaled with the amplitude of the [NADH] oscillations for comparison, but the fluorescence measurements of the CSTR experiments did not provide absolute values, unfortunately. Consequently, we can only compare the ratio of q_s for Glc_x and ACA_x. It is 5.3 in the model as compared to 11.3 in the experiments.

Thanks to the work of the Dutch group, we also know a number of oscillation amplitudes and phases approximately. The relative amplitudes of most of the metabolites also agree rather well with those determined in the batch experiments — especially when considering the rather large experimental errors (see Richard et al. [7] or compare the amplitudes of NAD^+ and NADH in Table 6). Still, the relative amplitudes of GAP, DHAP and ACA_x in the model are much smaller than observed experimentally. The phases relative to NADH are wrong. However, groups of related metabolites have similar errors in their phases relative to NADH. Thus, there is a phase change of $-12°$ from G6P to F6P in the model as compared to $-10°$ in the experiments, and the relative phases of FBP, ATP, ADP and AMP are also correct (as are NAD^+ and NADH as a consequence of a stoichiometric constraint). These facts might indicate an inherent difficulty with stopping all cellular reactions at exactly the same time in the experiments. It might also signal that NADH is not handled entirely correctly in the model, but the quenching phases relative to NADH do agree with the experiments.

Other local results are shown in Appendix C, and non-local results are presented in the following section.

8. Evaluation of the optimized kinetic equations

The optimization leading to the results presented in Section 7 has been strictly local in the sense that only properties of the system in an (arbitrary small) neighborhood of some stationary point have been considered. The fit is quite satisfactory as far as local properties go. However, the model is meant to apply more generally and consequently, we should evaluate it outside the special point used for the optimization, the bifurcating stationary point. Such evaluation may also serve as a check for the result of the optimization.

In this section we therefore study the model by numerical integration (using CHEM [52] based on CVODE [53]) and continuation [54,55] of the model kinetics, Eq. (7), for mixed flow concentrations of glucose and cyanide away from the bifurcation point. (For some integration packages for chemical kinetics, it is practical to implement Eq. (7) by changing the stoichiometric coefficients of the intracellular species to y_{vol} in each membrane reaction and divide the velocity parameter from Table 4 with y_{vol} for these.)

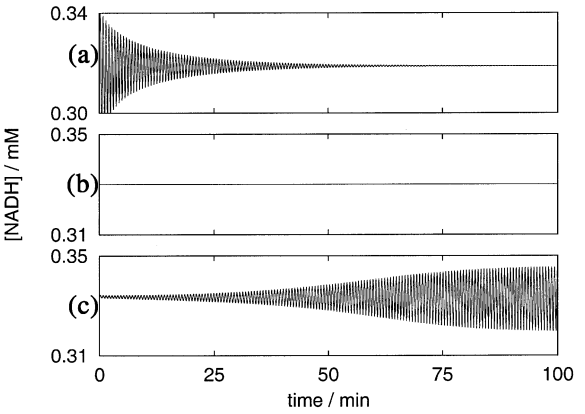

Fig. 4. Integration of the model before the Hopf bifurcation, at the Hopf bifurcation and after the Hopf bifurcation. The mixed flow concentration of glucose in mM, $[Glc_x]_0$, is: (a) 17.0; (b) 18.5; and (c) 20.0. All other parameters as indicated in Tables 4–7.

We first confirm explicitly that we do, in fact, have a supercritical Hopf bifurcation at $[Glc_x]_0 = 18.5$ mM. The results of the integration of the kinetic equations are shown for the concentration of NADH in Fig. 4: damped oscillations decaying to a stationary state for $[Glc_x]_0 = 17.0$ mM; a stationary state at the bifurcation value $[Glc_x]_0 = 18.5$ mM; and oscillations growing from an unstable stationary state towards a stable limit cycle for $[Glc_x]_0 = 20.0$ mM. (The change of stability of the stationary point can be demonstrated for an arbitrarily small interval around $[Glc_x]_0 = 18.5$ mM, but the change can be more easily seen if the interval is not too small.)

A more detailed representation of the change of behavior as the mixed flow glucose concentration is varied is presented in Fig. 5. Below the bifurcation, there is a stable stationary state, shown for the concentration of NADH (solid curve), which becomes unstable beyond the bifurcation (dashed curve). Beyond the bifurcation there also appear stable limit cycle oscillations, indicated as a 'profile', solid curves showing the minimum and maximum NADH concentrations during the oscillations. These two curves have vertical tangents in the bifurcation point, a behavior characteristic of a supercritical Hopf bifurcation where the amplitude grows as the square root of the bifurcation parameter. We shall return to that question shortly.

We note that the square root dependence applies approximately only in a (fairly small) interval beyond the bifurcation. For higher values of the mixed flow glucose concentration, the amplitude of the oscillations does not change much. This behavior agrees with the saturation of the glucose transporter observed in the experiments and, indeed, both the model and the experiments retain near-Hopf behavior for very large values of the mixed flow glucose concentration.

During limit cycle oscillations, all metabolites oscillate with the same frequency, but with different amplitudes and phases. Fig. 6 shows the oscillations of most of the metabolites at a mixed flow glucose concentration of 24 mM. This figure allows us to test the assumption, used in the optimization, that the mean intracellular metabolite concentrations at glucose saturation (in batch experiments) will be similar to those at the bifurcation point.

We find that the assumption holds true for all intracellular metabolites except Glc and Pyr, for which the average concentrations increase significantly as the mixed flow glucose concentration is increased (compare Fig. 6 and Table 6). No batch data were available on the intracellular glucose concentration, so this discrepancy is irrelevant to our optimization. Therefore, the only problem caused by this assumption is the pyruvate concentration. These considerations show that the use of concentration data from the batch experiments for the optimization of our model leads to a result

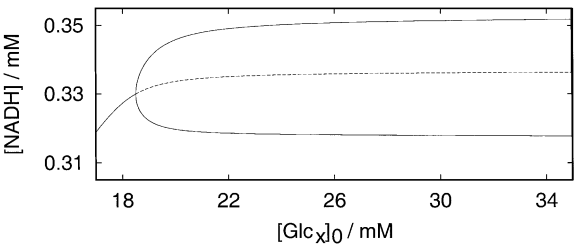

Fig. 5. Stationary point and profile of oscillations as functions of the mixed flow concentration of glucose, $[Glc_x]_0$. All other model parameters are as indicated in Tables 4, 5 and 7. See text for details.

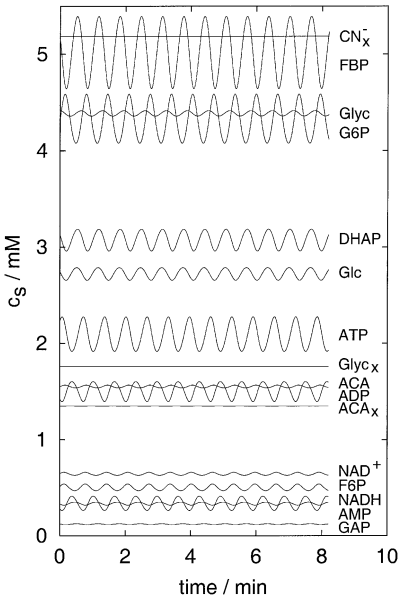

Fig. 6. Integration of the model at a mixed flow glucose concentration of $[Glc_x]_0 = 24.0$ mM. All other parameters as indicated in Tables 4, 5 and 7. The symbol c_s designates the concentration of species s. Mean values of concentrations of metabolites that do not fit in the figure are: $[Glc_x] = 6.7$ mM; [BPG] = 0.0003 mM; [PEP] = 0.041 mM; [Pyr] = 22 mM; [EtOH] 20 mM; and $[EtOH_x] = 17$ mM.

which — to a large extent — is self-consistent, thus justifying the approach.

Note that the cause of the specific problem with the mean pyruvate concentration can be explained simply by the kinetics: the K_M value of the PDC reaction is so low that the enzyme is practically saturated already at the bifurcation point, so even a minor increase in glycolytic flux will cause excessive pyruvate build-up. As indicated in Table 5, this particular K_M value was adopted initially from another glycolytic model because we were unable to find relevant biochemical data, and tentative changes did not improve the agreement of local properties. This exemplifies the importance of having realistic parameters for the optimization of models as large as this: in practice, it is impossible to predict all possible problems that might arise outside the local optimization as a consequence of a parameter set chosen.

The assumption of slow variation with the bifurcation parameter also holds for the relative amplitudes and phases. For most species, these are practically unchanged when the mixed flow glucose concentration is increased from 18.5 to 24 mM. The only exceptions are Glc_x and Glc. (At $[Glc_x]_0 = 24$ mM we have $a_{Glc_x} = 0.049 a_{NADH}$, $\theta_{Glc_x} = -160°$ and $a_{Glc} = 4.15 a_{NADH}$, $\theta_{Glc} = 30°$, relative to NADH.)

We may also use Fig. 6 to compare the absolute amplitudes of the different metabolites at $[Glc_x]_0 =$ 24 mM with those of the batch experiments [7]. We see that the amplitudes are generally much smaller in the model. This may be so because the instability does not grow fast enough with $[Glc_x]_0$ to reach a proper size of the limit cycle before the saturation of the glucose transporter sets in. So, this discrepancy may be caused by the biochemistry of the glucose transporter and by a rather low value of σ' or high value of $|g'|$ (see Table 9).

The CSTR experiments provide detailed data on the effect of increasing the mixed flow glucose concentration, which can be directly compared with the model. Sufficiently close to a supercritical Hopf bifurcation, the amplitude of the oscillations will grow as the square root of the distance from the bifurcation point, as we have said. So, by plotting the square of the amplitude as a function of the bifurcation parameter, we should get a curve with tangent in the bifurcation point of finite slope (neither infinite nor zero). Fig. 7a compares the square of the amplitude of the oscillations (defined here as half the difference between the maximum and minimum NADH concentration) as a function of the bifurcation parameter $[Glc_x]_0$. Because the NADH concentration is only known to within an unknown proportionality factor, we use a least squares fit for the ordinates.

As can be seen, Fig. 7a confirms the generic Hopf behavior close to the bifurcation point (tangent of finite slope) and the gradual, but rather sudden transition into the behavior resulting from the saturation of the glucose transporter. The prediction by the model is rather good. The bifurcation occurs at precisely the right value of $[Glc_x]_0$, but the saturation of the glucose transporter sets in too early in the model — the curve is initially too steep (and remember the fit for the scale of NADH concentrations).

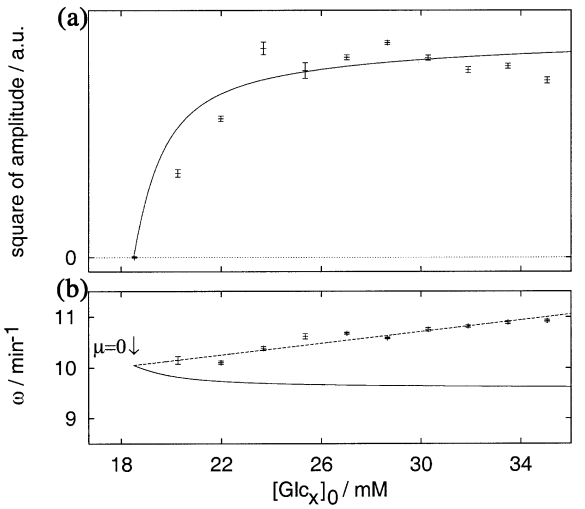

Fig. 7. Comparison with experiments [4]: square of amplitude (a) and angular frequency (b) vs. the mixed flow concentration of glucose, $[Glc_x]_0$. All other model parameters as indicated in Tables 4, 5 and 7. Discrete data points are from experiments, solid lines are model predictions and the dashed line in (b) is a fit of a straight line to the experimental data. Because the experimental NADH concentration is only known to within an unknown proportionality factor, we have used a least squares fit for the ordinates in (a). The abbreviation a.u. means arbitrary units.

The variation with $[Glc_x]_0$ of the frequency of the limit cycle oscillations is shown for the model and the experiments in Fig. 7b. They agree exactly at the bifurcation point, but the frequency decreases with $[Glc_x]_0$ in the model, whereas it increases in the experiments as discussed in the previous section. However, Fig. 7b shows that the frequency in the model remains close to the experimental value. For example, the period of oscillations at $[Glc_x]_0 = 24$mM is 36 s in the experiments whereas the model predicts 39 s.

The CSTR experiments provide similar bifurcation data for $[CN_x^-]_0$ as the bifurcation parameter (Fig. 1 in Section 3). The bifurcation diagram in Fig. 8 shows that the Hopf bifurcation at high $[CN_x^-]_0$ is found in both the model and the CSTR experiments, but at different mixed flow cyanide concentrations. The Hopf bifurcation at low $[CN_x^-]_0$ is not found in the model. However, this is to be expected since the initial effect of the cyanide is to block the respiratory chain of the mitochondria, which are not included in the present model. So, the model agrees qualitatively — but not quantitatively — with the solution diagrams presented in Section 3.

The bifurcation diagram indicates that a second region of oscillations exists in the model. However, there is no experimental evidence for the existence of such a region. Probably, it is an artifact which arises because the surface of Hopf bifurcations is crossed almost tangentially and therefore, happens to be intersected three times. This interpretation fits well with the observation that the value of σ' seems too low (see the discussion of absolute amplitudes above).

The model has already been compared with the quenching experiments in Table 6; in fact it was used in the optimization. However, that comparison applies to the bifurcation point and may be said to compare the behavior for infinitesimally small limit cycles. It is therefore of interest to compare the quenching behavior also for realistic, finite limit cycles.

We simulate a quenching experiment by integrating the limit cycle oscillations until some time for which the oscillation has the desired phase. Then, we shift the concentration of the metabolite added in the simulated experiment by any chosen value while keeping all the other concentrations fixed at the values they had at the point of the

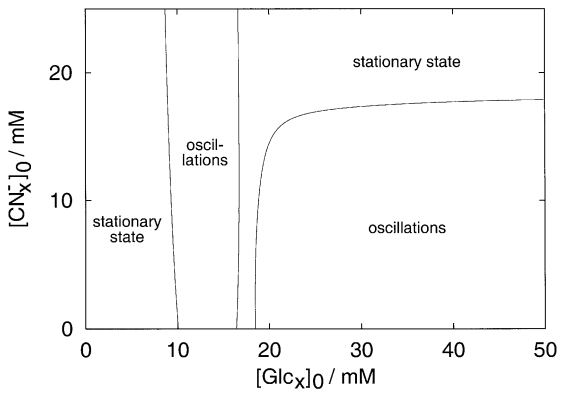

Fig. 8. Bifurcation diagram of the model. The mixed flow concentrations $[Glc_x]_0$ and $[CN_x^-]_0$ are used as bifurcation parameters as in the CSTR experiments. All other parameters as indicated in Tables 4, 5 and 7.

simulated addition. We then continue the integration with the new set of concentrations as initial values. The phase and concentration change to be used in order to quench the oscillations is unique and must be determined by trial and error, but the values calculated at the bifurcation point form excellent initial guesses, so the correct quenching data for the simulation are not hard to find.

So in order to simulate an 'actual' quenching experiments with addition of Glc_x or ACA_x as described above, we must integrate the kinetic equations away from the bifurcation point. In the quenching with ACA_x, we work at the experimental operating point. The quenching with Glc_x can only be performed when the glucose transporter is not saturated. (This is true both in the model and in the experiments.) As just mentioned, the saturation occurs somewhat too early in the model, so the glucose quenching cannot be performed exactly at the working point of the experimental quenching. Instead, we work at a point where the degree of saturation is comparable to that in the experiment.

Fig. 9 shows the results of these simulations. In panel (a), the concentration of extracellular glucose, $[Glc_x]$, is suddenly changed by 4.49 mM at a phase of $-3°$, close to experimental quenching phase of 4°, resulting in quenching of the oscillations. (In the experiments, 1.11 mM of Glc_x was needed to quench the oscillations in a comparable, but not identical, working point.) Panel (b) shows the simulation of the experimental quenching by addition of ACA_x with a change of concentration of 0.3 mM at a phase of $-170°$. This should be compared with the experimental quenching obtained by adding 0.098 mM ACA_x at 172°.

The simulated quenching with ACA_x may be compared with panel (c), which shows the result of the same instantaneous concentration change at the opposite phase. Whereas (a) and (b) show successful quenchings, (c) shows instead a small increase of the instantaneous amplitude, thus exemplifying the characteristic phase dependence of the response. Summarizing, the quenching phases differ from the experimental values by -7 and 18°, respectively, and the quenching concentrations differ by factors of four and three, respectively, for Glc_x and ACA_x.

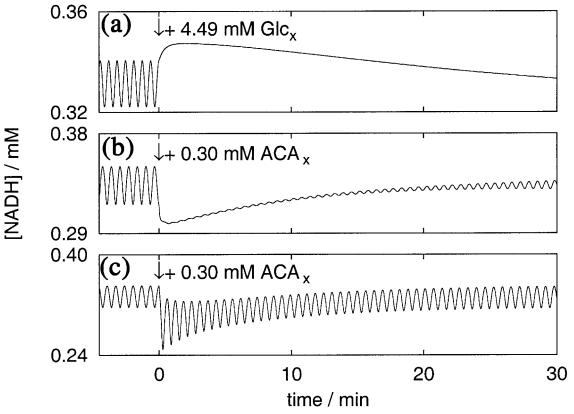

Fig. 9. Simulations of perturbations with Glc_x and ACA_x (arrows indicate time of perturbations). (a) Quenching with Glc_x at $-3°$ — mixed flow glucose concentration $[Glc_x]_0 = 19.0$ mM, mixed flow cyanide concentration $[CN_x^-]_0 = 5.6$ mM, and specific flow rate $k_0 = 0.048$ min^{-1}. (b) Quenching with ACA_x at $-170°$ — $[Glc_x]_0 = 35.0$ mM, $[CN_x^-]_0 = 5.37$ mM, and $k_0 = 0.0479$ min^{-1}. (c) ACA_x perturbation at 10° [operating conditions as in panel (b)]. All other parameters as indicated in Tables 4, 5 and 7. Compare with Fig. 10 in Appendix C.

Fig. 9a,b should be compared with the experimental quenchings in Fig. 10 in Appendix C. We note the presence of slow non-oscillatory transients in the model results. The one for acetaldehyde agrees qualitatively with the one seen in the experiments. This behavior is due to the excitation of one or more of the slow stable monotonous (non-oscillatory) modes (see the table of eigenvalues in Appendix C). The non-oscillatory transient seen in the model quenching with glucose is not present in the experiments. Comparison also shows that the spiraling return to the limit cycle is too slow in the model. Again, this points to too low a value of σ' or too high a value of $|g'|$.

As discussed in Section 3, the experiments suggest that the synchronization of the yeast cells is strong. In fact, this is what allows us to use macroscopic data in the optimization as if the data applied to a single cell. It is straightforward to extend the present model, so that it describes two (identical) cells and a common extracellular phase (see Wolf and Heinrich [20,23]). We have integrated this 35-dimensional extended model with various initial conditions and at various operating

points of the CSTR. In all cases tested, we found that the stable solution is synchronized with the two cells oscillating in opposite phases, and that the in-phase synchronization is unstable.

Furthermore, the synchronization process seems to be an order of magnitude too slow. So, the present model (extended as indicated) cannot simulate Pye's mixing experiment [6,18,19], and there is a lack of self-consistency in that the model cannot reproduce the strong coupling seen in the experiments. In principle, the entire optimization could have been performed on the extended model without introducing additional parameters. This way, the question of synchronization phase could have been addressed along with the other local properties at the bifurcation point. However, we have not pursued this point any further.

9. Discussion

Despite its many desirable features, the present model has a number of limitations. First of all, it builds on a fixed, pre-assigned set of functional forms for the rate equations, some of which lack conclusive biochemical justification. The variation in functional form can easily be handled with the present method, however, e.g. by including several proposed forms for a reaction in one single parametrized expression. Besides biochemical limitations, progress along this line is impeded by the increase in the effective dimension of the parameter space to be searched.

The magnitude of the computational problem is already a major issue even without variation of functional forms; the number of points to be analyzed grows exponentially with the number of parameters to be searched. It is simply impossible to test all relevant combinations of unknown parameters reasonably densely by brute force in a system as large as the present one. This also means that the resulting model, exhibited in Section 7, is not necessarily the best possible solution for the given set of functional forms. We cannot exclude that a better model exists for parameter combinations that have not been tested.

This situation could be improved with a combination of several measures. The most obvious one is to use fast parallel computation and methods to handle large sets of data efficiently. (The problem parallelizes perfectly.) Another area is improvement of mathematical and numerical algorithms and search strategies. But really decisive improvements can only come through new or more accurate biochemical data.

An important feature of the optimization is that it is local, i.e. concerned with properties in one point of concentration space. This is essential to the method, but it also limits the properties that can be taken into account. Nevertheless, the resulting model also gives sensible predictions when used away from the point of optimization — although only some neighborhood of that point has been considered. The model has not been tested at widely different conditions since we have no experimental data to compare with.

Yet another limitation is that the model is based on a two-phase approximation to the cell suspension. This means that synchronization between oscillations in different cells is assumed from the beginning. The consistency of this assumption can be tested by extending the optimized model as described in Section 8, and as shown there, two cells running glycolysis according to the model fail to synchronize in phase: they synchronize in antiphase, and much too slowly.

The current hypothesis of cell synchronization in yeast cells is that ACA_x mediates the synchronization [6]. So the absence of significant oscillations in any of the extracellular species (see Table 6 and Fig. 6) 'explains' the very slow synchronization seen in our model. Despite a considerable effort, we were unable to make the model reproduce the rather large amplitude of the oscillations of ACA_x reported by Richard et al. [6]. We must conclude that the question of synchronization remains an unsolved problem of the modeling (compare also Wolf and Heinrich [23] and Winfree [24], p. 297).

The optimization of a system with many unknown parameters requires a large set of data, and the present work builds on extensive dynamical data. In the present study, a large part of these are associated with the glycolytic oscillations. However, possible local dynamical properties and methods to obtain them are not limited to the ones described here. As alternatives, we call attention

to Eigen's relaxation kinetics [56], the various methods described in Chevalier et al. [57] and Stemwedel et al. [58], and the very general method of 'Kinetic spectrometry' [48] (when fully developed experimentally).

Even without dynamical data, the direct method may provide valuable guidance in establishing a model because biochemical pathways often have few branchings. So if enough metabolite concentrations and Michaelis constants are known, the set of possible maximum velocities can be obtained, and parametrized by a few parameters. Nevertheless, the promise of the method lies in combining results of mechanistic biochemical work and dynamical experiments.

Because of the limitations discussed above, the model should be viewed first of all as a step toward a complete, quantitative description of glycolysis that can be used for predicting the dynamical behavior under other conditions and the effect of specific mechanistic changes. For the present model, one should keep in mind that inaccuracies in one rate equation might lead to incorrect interpretations of the effect of changes of rate equations for other steps.

10. Conclusion

The optimization method described in this paper can provide a solution to the fundamental problem of modeling an entire pathway accurately. We have shown this by developing a full-scale model of glycolysis in *Saccharomyces cerevisiae* with an unprecedented degree of biochemical and dynamical realism, as evidenced by the tables and figures of Sections 7 and 8.

The method works at a stationary point, and a characteristic feature is that biochemical properties of the model on a system level like metabolite concentrations and metabolic fluxes, can be assigned their experimental values from the outset. Maximum velocities are eliminated from the problem, but are calculated (for the optimum model only) at the end of the optimization. The method avoids integration of kinetic equations; calculation of dynamical properties is the only time-consuming operation.

The resulting model embodies our current understanding of glycolysis in yeast in concise mathematical form by linking a mechanistic description, firmly based on biochemical data, with a quite accurate representation of the measured properties of the system as a whole.

A vast body of biochemical data from different sources exists for other pathways, which could be integrated into models if extended with dynamical measurements. Indeed, extensive biochemical and dynamical measurements combined with the direct method, may bring the final goal of building a faithful model of a pathway like glycolysis within reach, when the optimization is extended to include variation of the functional forms of unsettled rate equations. The present work may serve as a guide to such use of the method.

Acknowledgements

The authors would like to acknowledge the importance of the experimental work on yeast cells by the Dutch group. Without their extensive set of data, the present optimization would not have been possible.

Appendix A: Biochemical abbreviations

Enzymes:

ADH:	alcohol dehydrogenase
AK:	adenylate kinase
ALD:	aldolase
ENO:	enolase
G3PDH:	glycerol 3-phosphate dehydrogenase
GAPDH:	glyceraldehyde 3-phosphate dehydrogenase
HK:	hexokinase
PDC:	pyruvate decarboxylase
PFK:	phosphofructokinase-1
PGI:	phosphoglucoisomerase
PGK:	phosphoglycerate kinase
PGM:	phosphoglycerate mutase
PK:	pyruvate kinase
TIM:	triosephosphate isomerase

Metabolites:

ACA:	intracellular acetaldehyde
ACA_x:	extracellular acetaldehyde
ADP:	adenosine 5′-diphosphate

AMP: adenosine 5′-monophosphate
ATP: adenosine 5′-triphosphate
DHAP: dihydroxyacetone phosphate
BPG: 1,3-bisphosphoglycerate
EtOH: intracellular ethanol
$EtOH_x$: extracellular ethanol
F6P: fructose 6-phosphate
FBP: fructose 1,6-bisphosphate
G6P: glucose 6-phosphate
GAP: glyceraldehyde 3-phosphate
Glc: intracellular glucose
Glc_x: extracellular glucose
Glyc: intracellular glycerol
$Glyc_x$: extracellular glycerol
NAD^+: nicotinamide adenine dinucleotide (oxidized form)
NADH: nicotinamide adenine dinucleotide (reduced form)
PEP: phosphoenol pyruvate
Pyr: pyruvate
UTP: uridine 5′-triphosphate

Appendix B: Stationary reaction velocities

In Section 5.1, we obtained the representation [Eq. (5)] of a stationary net velocity for the model of glycolysis in terms of extreme currents on the basis of biochemical arguments. A similar procedure is often possible with other biochemical pathways. But for complicated reaction networks, such an approach may not be feasible. In this case, the extreme currents can be found systematically by solving sets of linear equations derived from the stoichiometric matrix. In this appendix, we show that the set of all stationary reaction velocities has a simple geometry in which the extreme currents play a special role that allows us to express any stationary velocity in terms of them. We show how they can be calculated.

The use of these ideas in chemistry was pioneered by Clarke [47] in the context of stability of chemical networks, and we shall refer to the mathematical treatment in Clarke [47], chapter II, Section C, for proofs and technical details. For visualization of the geometrical objects and their relation to chemistry, low dimensional chemical examples can be helpful, and we refer to Hynne et al. [2,3], especially the figures and tables therein.

A stationary state is characterized by time independent concentrations, $\dot{\mathbf{c}} = \mathbf{0}$, but the condition for stationarity is most simply expressed in terms of velocities, which are time independent as well. Any stationary reaction velocity is mapped to zero by the stoichiometric matrix, as Eq. (2) shows. (The factor y_s on the left is different from zero for all s, so any non-stationary velocity is mapped to a non-zero vector.) This means that stationary velocity vectors lie in the null space, N, of the stoichiometric matrix, $\boldsymbol{\nu}$,

$$\boldsymbol{\nu}\cdot\mathbf{v} = \mathbf{0}, \tag{9}$$

and non-stationary velocity vectors lie outside N.

We first clear up a minor technical detail arising if we work in terms of net reaction velocities. Any stationary net reaction velocity is mapped to zero by the stoichiometric matrix for the forward reactions. Thus, we get essentially the same formalism whether we work with net reactions or separate forward and reverse reactions, and for simplicity of discussion, we shall talk about velocities and comment when there are differences. The results can be interpreted in terms of net velocities, which is most relevant to the discussion in Section 5.1.

Since reaction velocities are non-negative, all stationary velocities lie in the intersection of the null space of the stoichiometric matrix, N, and the non-negative orthant of velocity space (where all components of any vector are positive or zero). The null space is a subspace of velocity space, so the intersection is a convex polyhedral cone with apex at the origin of the coordinate system. Its cross-section is a polytope (finite convex polyhedron) [47,59], which can be obtained as the subset of the cone, for which the sum of components of vectors have a given, fixed value. We shall follow Clarke [47] and refer to the cone and polytope as the current cone and current polytope. (Recall that current is short for stationary velocity vector.)

It is helpful to visualize the geometry of cone and associated polytope in three-dimensional space as in the figures of Hynne et al. [2,3]. A three-dimensional cone would perhaps be better described as a pyramid (extending to infinity) with definite edges. A cross-section of such a three-

dimensional pyramid is a convex polygon (a two-dimensional polytope), and a vector from the origin to a vertex of the polygon lies along the corresponding edge of the pyramid (cone). A higher dimensional current cone can similarly be characterized by its edges or by vectors from the origin to the vertices of its cross-section, the current polytope.

These vectors, $\mathbf{E}_i$, along the edges of the current cone are the extreme currents. The term 'extreme' seems intuitively reasonable, and the vertices of a current polytope are extreme points in the sense of the theory of convex sets [59]. Quite generally, any stationary reaction velocity, **v**, can be represented by a point in the current cone and expressed as a linear combination with non-negative coefficients, j_i of the extreme currents $\mathbf{E}_i$:

$$\mathbf{v} = \sum_i j_i \mathbf{E}_i. \tag{10}$$

(This property follows from the convexity of the current cone, which again follows from the convexity of the intersection of two convex sets as mentioned above.)

Eq. (10) is the general expression for the stationary reaction velocity, which (together with the set of all possible metabolite concentration vectors and intrinsic kinetic constants) can be used for a scan over all possible models in all possible stationary states. There are three issues we need to discuss in order to be able to use Eq. (10) in practice in the general case.

We first note what may happen if we work in terms of net velocities as in Eq. (5). Net reaction velocities may sometimes be negative for a network and, in this case, the geometrical interpretation above must be modified. However, we may always avoid the problem by including forward and reverse velocities explicitly for those reversible reactions that may have negative net velocities.

The second issue is how to actually calculate the extreme currents $\mathbf{E}_i$ to use in Eq. (10) for a scan. To get the set of all possible extreme currents we must solve a set of linear equations with a matrix obtained from the stoichiometric matrix by selecting sets of $n+1$ columns in all possible ways (with n the number of independent species) supplemented with a normalization condition. Each extreme current may be obtained several times this way. The procedure is described in more detail (and justified in geometrical terms) by Clarke [47], page 23.

The third practical issue concerns efficiency. Although any stationary reaction velocity can be obtained as a linear combination [Eq. (10)], the representation is only unique if the polytope is a 'simplex'. Otherwise, if we scan all possible linear combinations [Eq. (10)], we cover the cone several times, leading to a considerable waste of computational resources. The best solution in this case is to partition the polytope into simplices, and scan each of the corresponding cones in turn.

A current polytope is a simplex when the number of extreme currents equals $m-n$, the difference between the number of independent reactions, m, and the number of independent species, n. In this case, the endpoints of the extreme currents form the vertices of a current polytope, regardless of normalization. If there are more than $m-n$ extreme currents, their endpoints do not in general define a current polytope unless they are suitably normalized, e.g. so that the sum of components equals a given fixed value. For the purpose of optimization it is not necessary to normalize extreme currents in this way, however.

We conclude this appendix with a brief discussion of how the general theory applies to our glycolysis model. Here all net velocities are non-negative at stationarity, so we can use the general description for the net velocities. The net current cone is four-dimensional but can be understood in terms of its cross-section, the net current polytope, which is a tetrahedron. This is a simplex, in agreement with the fact that we have 24 forward reactions and 20 species; thus, the difference (four) equals the number of extreme net currents. The extreme net currents (Table 3), which are velocities of the four irreducible subpathways (Fig. 3) form the four edges of the net current cone, and the endpoints of these vectors are the vertices of the tetrahedron. Since a tetrahedron is a simplex, there is no problem of redundancy here; Eq. (10) can be used as it stands for the scanning.

Appendix C: Dynamical properties of the model

A model as large as the one studied here can be cumbersome to work with. However, the dynamics of the model near the stationary point at or near the Hopf bifurcation can be described quite well by the linearization of the kinetic equations with additional non-linearities for the bifurcating modes. We have already presented some dynamical properties of the optimized model in the tables of Section 7. In this appendix, we give a more complete account of the dynamics and the background for the dynamical results cited in the main text.

In simplest terms, the dynamics of the system near the bifurcating stationary state is described by the eigenvalues and eigenvectors of the Jacobi matrix. Of these, we have quoted the angular frequency ω_0 of the oscillations in Table 9, and the amplitudes and phases together with q_s quenching concentrations and quenching phases for each metabolite in Table 6. These quantities are all related to eigenvalues and eigenvectors associated with the oscillating mode; ω_0 is the imaginary part of the eigenvalue, amplitudes and phases are related to the right eigenvector and the quenching data are related to the left eigenvector (one of the two complex conjugate vectors), as described in Section 2.4.

The spectrum of eigenvalues of the Jacobi matrix is shown in Table 10. In the present model, there is only one pair of complex conjugate eigenvalues (which are pure imaginary because we are exactly at the Hopf bifurcation point). All other eigenvalues are real. The reciprocal of a real eigenvalue is a characteristic time for the exponential motion in the associated mode. All real eigenvalues in Table 10 are negative indicating stability (decaying exponentials) for those modes. We note that there are several very slow real modes with characteristic times of approximately 20 min, and very fast modes with characteristic times down to approximately 0.1 ms. Away from the bifurcation point, the reciprocal of the real part of a complex eigenvalue is a characteristic time associated with changes in amplitude of the oscillatory motion near the stationary point, whereas $2\pi/\omega_0$ is the period of oscillation at the bifurcation, 0.625 min. The species involved in the various modes and the degree of their variation are determined by the right eigenvectors. However, apart from those associated with the oscillations already given implicitly in Table 6, we shall not present the extensive tables of these eigenvectors.

Whereas a linear approximation is usually adequate for most modes, non-linear terms are always important for a bifurcating mode where the real part of an eigenvalue vanishes at the bifurcation point. For the oscillations near the Hopf bifurcation, we need non-linear terms to account for the existence of a limit cycle and the way it grows with a bifurcation parameter and, in particular, to

Table 10
Eigenvalues of the Jacobi matrix at the bifurcation

$10.05i$	−0.06918	−17.00	−620
$-10.05i$	−0.1119	−32.48	−1289
−0.04718	−0.1993	−63.08	−1873
−0.04720	−1.933	−75.41	−3402
−0.05082	−2.771	−174.7	−725 800

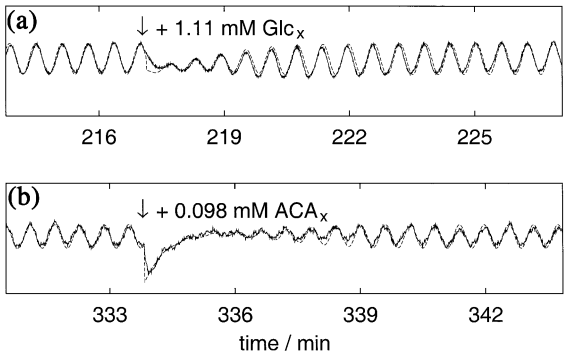

Fig. 10. Fit of a Hopf normal form with two slow modes (dashed lines) to time series from quenching experiments [4]. Differences in perturbation response arise because perturbations with different metabolites excite the slow modes differently. (a) Quenching of the oscillations by addition of 1.11 mM Glc_x at 4°. The cell density is 1.62×10^9 cells/ml, $[Glc_x]_0=23.1$ mM, $[CN_x^-]_0=4.26$ mM, and $k_0=0.0506$ min^{-1}. (b) Quenching of the oscillations by addition of 0.098 mM ACA_x at 172°. The cell density is 1.66×10^9 cells/ml, $[Glc_x]_0=35.0$ mM, $[CN_x^-]_0=5.37$ mM, and $k_0=0.0479$ min^{-1}. In both fits $r_{lc}^2 g'=-0.857$ min^{-1}, $r_{lc}^2 g''=-0.176$ min^{-1} and the relaxation times of the slow modes are 0.583 and 1.33 min, respectively. In each of the fits ω_{lc} is adjusted according to Fig. 7b. See Danø et al. [82] for details of the fitting.

determine whether the bifurcation is supercritical or subcritical. These problems are best dealt with through a systematic description of the oscillating mode in terms of a normal form representation, which we now briefly describe.

The complete dynamics of the model is embodied in the kinetic equations, but the oscillatory modes can be faithfully described much more simply in terms of a differential equation in one complex variable, z, which we shall refer to as a (complex) amplitude:

$$\dot{z} = (i\omega_0 + \sigma\mu)z + g|z|^2 z + ... \quad (11)$$

[The amplitude in Eq. (11) is often written with g replaced by $-g$ in the literature.] The behavior of the actual biochemical system is then described in terms of concentrations through a transformation of the solution $z(t)$ to Eq. (11) from the complex plane of amplitudes to concentration space, namely

$$\mathbf{c} = \mathbf{c}^* + \mathbf{h}_{001}\mu + 2\mathrm{Re}(\mathbf{u}z + \mathbf{h}_{200}z^2) + \mathbf{h}_{110}|z|^2 + ... \quad (12)$$

in which $\mathbf{u}$ is the right eigenvector corresponding to the pair of complex eigenvalues, and the coefficients $\mathbf{h}$ are given in Table 11.

Table 11
Transformation parameters for transformations between the normal form description and the full model (see text for details)

Species	$\mathbf{h}_{001}$ (mM)	$\mathbf{h}_{110}$ (mM)	$\mathrm{Re}\mathbf{h}_{200}$ (mM)	$\mathrm{Im}\mathbf{h}_{200}$ (mM)
Glc_x	0.6919	91.8600	0.1928	−0.0252
Glc	0.3683	43.3700	−12.5000	6.2270
G6P	0.0830	120.1000	120.8000	−21.7900
F6P	0.0088	16.7400	19.3800	4.3450
FBP	0.3050	−55.2700	−140.4000	63.4800
GAP	0.0037	−1.2560	−2.1200	1.0670
DHAP	0.1013	−36.9500	−40.5600	36.0400
BPG	0.0000	−0.0010	0.0149	0.0211
PEP	0.0008	−0.3478	−0.2196	0.0409
Pyr	4.4000	−2242.0000	−10.1500	20.4900
ACA	0.0541	−17.4900	8.2480	−4.3670
EtOH	0.2866	−159.6000	−8.8270	7.2660
$EtOH_x$	0.2451	−136.5000	0.1004	0.1261
Glyc	0.1509	−48.8100	1.0610	6.5750
$Glyc_x$	0.0606	−19.6000	0.0105	−0.0017
ACA_x	0.0471	−15.2400	−0.0868	−0.1739
CN_x^-	−0.0135	4.3570	0.0001	−0.0001
ATP	−0.0042	−113.4000	80.2100	46.8700
ADP	0.0025	26.1500	−50.1100	−47.7500
NADH	0.0044	−1.0920	−8.9450	−0.5284

In this way, we describe the actual behavior of the concentration of each of the 20 metabolites in terms of two-dimensional dynamics [Eq. (11)]. All the complications of the high-dimensional concentration space is contained in the transformation [Eq. (12)], which is independent of time.

The parameters of Eqs. (11) and (12) can be calculated from the kinetic equations using formulae given in Ipsen et al. [34] (see also, e.g. [33,60]). In Eq. (11), μ is a bifurcation parameter which is zero at the bifurcation (see Section 2). In the present model, μ is defined as the dimensionless quantity $\mu = ([Glc_x]_0 - [Glc_x]_0^*)/\mathrm{mM}$, in which $[Glc_x]_0$ is the mixed flow concentration of extracellular glucose and $[Glc_x]_0^*$ is its value at the bifurcation point. From an experimental point of view, this is the obvious choice of bifurcation parameter since this is the parameter varied in the CSTR experiments. However, because the saturation of the glucose transporter makes the oscillations in the cells insensitive to changes of μ already quite close to the bifurcation point, the linear μ-dependence of Eq. (11) applies only in a rather narrow interval beyond the bifurcation. (Contributions to the amplitude equation of higher orders in μ or a 'better' choice of bifurcation parameter would extend the range of applicability.)

The parameters σ and g are complex and can be expressed in terms of their real and imaginary parts as $\sigma = \sigma' + i\sigma''$ and $g = g' + ig''$. The parameter σ determines how fast the eigenvalue ($i\omega_0$ at the bifurcation) changes with the bifurcation parameter, so σ' is the growth rate of the instability and σ'' is the rate of change of the frequency near the stationary point. The real part g' of the coefficient g of the cubic term in Eq. (11), determines whether the bifurcation is supercritical, $g' < 0$, or subcritical, $g' > 0$; Table 9 shows that the Hopf bifurcation is supercritical in the optimized model. Together with σ' it determines the amplitude of the limit cycle oscillations in the complex z-plane as

$$r_{\mathrm{lc}} = \sqrt{\frac{-\sigma'\mu}{g'}} \quad (13)$$

which determines the limit cycle amplitude of each

metabolite through the transformation, Eq. (12). The parameters σ and g together determine the frequency of the limit cycle oscillations as well:

$$\omega_{lc} = \omega_0 + \left(\sigma'' - \frac{\sigma' g''}{g'}\right)\mu \qquad (14)$$

(which should be distinguished from the frequency of oscillations near the stationary point, $\omega_0 + \sigma''\mu$). The results Eqs. (13) and (14) follow from Eq. (11), which is the lowest order of expansions in z, $\bar{z}$ and μ[4]. The parameters σ and g can be calculated from expressions given in Table II of Ipsen et al. [34] where σ and g are denoted σ_1 and g_3. Their values for the model of glycolysis are given in Table 9. Note that the complex amplitude is defined dimensionless.

We can sometimes obtain experimental estimates of the normal form parameters, g' and g'', associated with a cubic non-linearity and σ' and σ'' associated with the linear stability through the dependence of the limit cycle amplitude and frequency on the bifurcation parameter [Eqs. (13) and (14)], or through perturbation experiments. Fig. 10 shows a fit of a normal form solution extended with two slow exponential modes to the responses following experimental quenching events. Unfortunately, we can only exploit part of this information for comparison as shown in Table 9, because the measurements only give r_{lc} up to an unknown proportionality constant.

The transformation in Eq. (12) is defined in terms of parameters whose real and imaginary parts are vectors in concentration space. (The eigenvector $\mathbf{u}$ and the coefficient $\mathbf{h}_{200}$ are complex, whereas $\mathbf{h}_{001}$ and $\mathbf{h}_{110}$ are real as is $\mathbf{c}^*$.) The $\mathbf{h}$ coefficients are exhibited in Table 11, whereas the stationary point $\mathbf{c}^*$ is given explicitly in Table 6, and $\mathbf{u}$ can be obtained from the oscillation amplitude and phase given in Table 6 as $u_s = a_s \exp(-i\theta_s)$ for the s component of $\mathbf{u}$. The amplitude and phase are given in Table 6 relative to those of NADH, and the same convention is used in the normalization of $\mathbf{u}$. As an example, we may calculate the amplitude of the [NADH] oscillations in the limit cycle for $\mu = 0.1$ ($[\mathrm{Glc}_x]_0 = 18.6$ mM):

$$a(\mathrm{NADH}) = \sqrt{\frac{-\sigma'\mu}{g'}} \times 2\mathrm{Re}(\mathrm{u(NADH)}) = 0.00454 \text{ mM} \qquad (15)$$

in the linear approximation of the transformation (for which the concept of an amplitude is best defined), which agrees with the result of direct integration: $a(\mathrm{NADH}) = 0.00446$ mM. For G6P, the normal form predicts an amplitude of 0.0718 mM as compared to 0.0705 mM in the integration of the full model. The frequency of the limit cycle oscillations for $[\mathrm{Glc}_x]_0 = 18.6$ mM ($\mu = 0.1$) calculated from Eq. (14) to $\omega = 10.0311$ min^{-1}, in good agreement with the result of integration 10.0312 min^{-1} (which has changed a little from the value of $\omega = 10.0505$ min^{-1} for the model at the bifurcating stationary point).

The normal form results are truncations of systematic expansions and apply only sufficiently near the bifurcation. In particular, they do not account for the saturation observed at higher values of $[\mathrm{Glc}_x]_0$. To appreciate the significance of the terms of the transformation and the associated coefficients of Table 11, we can relate the last row of Table 11 for NADH to figures of Section 8. The term $\mathbf{h}_{001}\mu$ corrects for the shift of the stationary point with μ to lowest order in μ. Thus, from Table 11, we see that the slope of the curve for the stationary NADH concentration as a function of the bifurcation parameter in Fig. 5 has a slope of 0.0044 in the bifurcation point.

The term $\mathbf{h}_{110}|z|^2$ can be used to calculate how much the average value of the oscillatory concentration deviates from the stationary point (depending on the amplitude) to lowest order. From Table 11, we can see that the term is negative, which may be barely visible in Fig. 5 very close to the bifurcation point. The term of Eq. (12) in $\mathbf{h}_{200}$ accounts for the second harmonic contribution to the oscillations. The term is complex and adds to the linear term (which is also complex) before the real part is taken, so the precise change of waveform depends on phase relationships as well as magnitudes. The truncated form can be used only close to the bifurcation point, so it is not quite applicable to Fig. 6. Nevertheless, we may note the small anharmonicity in the [NADH] oscillations in Fig. 6.

[4] (A bar over a symbol denotes complex conjugation).

Eq. (11) effectively describes the oscillations in two dimensions (one complex variable), and the transformation [Eq. (12)] translates the motion in the complex z-plane to the actual motion on a two-dimensional surface in concentration space, which approximately describes the oscillatory motion in the neighborhood of the unstable stationary point and the stable limit cycle for bifurcation parameters in an interval near the Hopf bifurcation.

The reduction from 20 to two dimensions is a very significant simplification. Yet, the oscillations are described *quantitatively correct* (if approximate) by the two-dimensional solution. The computational efficiency can be further increased by extracting the basic oscillations near the stationary state at the bifurcation as described in Kuramoto [60] or section VI of Ipsen et al. [34]. Solutions to the modified equation shows oscillations with slowly varying amplitude and phase, which can be integrated much more effectively. The simple Eq. (11) (modified or not) can be integrated in closed form, but similar equations arise for spatial reaction–diffusion systems, e.g. which cannot be integrated analytically. Here, a description in terms of a slowly varying amplitude can sometimes reduce computation time by a factor of 1000 or more.

Near a supercritical Hopf bifurcation the amplitude of oscillations always changes slowly (and becomes constant at the limit cycle), and, in this sense, the motion is slow. If the real parts of all other eigenvalues of the Jacobi matrix (evaluated at the stationary state at the bifurcation) are negative and numerically much larger than $\sigma'\mu$ at the point of operation, the time development of the system will be well described by Eqs. (11) and (12) after a short transient (when the initial state is not too far from the limit cycle).

However, the eigenvalues of the Jacobi matrix for the optimized model has several very slow modes in addition to the oscillations considered. Consequently, Eqs. (11) and (12) may not be adequate for a description of the local dynamics of the system when non-oscillatory modes can be excited, except very close to the bifurcation. It is possible to find other normal forms describing oscillations with several additional slow modes as in Ipsen et al. [61], but a discussion is outside the scope of this paper.

The normal form description with slow modes can be used directly with the experimental data to express the understanding that the system has the universal behavior of a system close to a Hopf bifurcation. This is demonstrated by the fit of a Hopf normal form to two experimental quenchings shown in Fig. 10. This way, normal form parameters can be estimated directly from the experiments and used to model yeast cell dynamics. In this case, however, the transformation from the normal form to the concentration space (Eq. (12)) would be unknown, and the distance μ from the bifurcation point would be undefined.

The normal form describes how a single oscillator behaves close to a Hopf bifurcation, so the fact that this gives a good description of our system (which has on the order of one billion cells) is an indication that it is indeed sensible to describe it as synchronized cells close to a Hopf bifurcation, and thus to model it as a two-phase system.

References

[1] B. Teusink, I. Passarge, C.A. Reijenga, et al., Can yeast glycolysis be understood in terms of *in vitro* kinetics of the constituents enzymes? Testing biochemistry, Eur. J. Biochem. 267 (2000) 5313–5329.

[2] F. Hynne, P.G. Sørensen, T. Møller, Current and eigenvector analyses of chemical reaction networks at Hopf bifurcations, J. Chem. Phys. 98 (1993) 211–218.

[3] F. Hynne, P.G. Sørensen, T. Møller, Complete optimization of models of the Belousov–Zhabotinsky reaction at a Hopf bifurcation, J. Chem. Phys. 98 (1993) 219–230.

[4] S. Danø, P.G. Sørensen, F. Hynne, Sustained oscillations in living cells, Nature 402 (1999) 320–322.

[5] P. Richard, J.M. Diderich, B.M. Bakker, B. Teusink, K. van Dam, H.V. Westerhoff, Yeast cells with a specific cellular make-up and an environment that removes acetaldehyde are prone to sustained glycolytic oscillations, FEBS Lett. 341 (1994) 223–226.

[6] P. Richard, B.M. Bakker, B. Teusink, K. van Dam, H.V. Westerhoff, Acetaldehyde mediates the synchronization of sustained glycolytic oscillations in populations of yeast cells, Eur. J. Biochem. 235 (1996) 238–241.

[7] P. Richard, B. Teusink, M.B. Hemker, K. van Dam, H.V. Westerhoff, Sustained oscillations in free-energy state and hexose phosphates in yeast, Yeast 12 (1996) 731–

740.
[8] B. Teusink, C. Larsson, J. Diderich, et al., Synchronized heat flux oscillations in yeast cell populations, J. Biol. Chem. 271 (1996) 24442–24448.
[9] E.E. Sel'kov, Self-oscillation in glycolysis. A simple kinetic model, Eur. J. Biochem. 4 (1968) 79–86.
[10] A. Goldbeter, Biochemical Oscillations and Cellular Rhythms, Cambridge University Press, Cambridge, 1996.
[11] O. Richter, A. Betz, C. Giersch, The response of oscillating glycolysis to pertubations in the NADH/NAD system: a comparison between experiments and a computer model, Biosystems 7 (1975) 137–146.
[12] Y. Termonia, J. Ross, Oscillations and control features in glycolysis: numerical analysis of a comprehensive model, Proc. Natl. Acad. Sci. USA 78 (1981) 2952–2956.
[13] C.G. Hocker, I.R. Epstein, K. Kustin, K. Tornheim, Glycolytic pH oscillations in a flow reactor, Biophys. Chem. 51 (1994) 21–35.
[14] K. Nielsen, P.G. Sørensen, F. Hynne, H.-G. Busse, Sustained oscillations in glycolysis: an experimental and theoretical study of chaotic and complex periodic behavior and of quenching of simple oscillations, Biophys. Chem. 72 (1998) 49–62.
[15] J. Babul, D. Clifton, M. Kretschmer, D.G. Fraenkel, Glucose metabolism in *Escherichia coli* and the effect of increased amount of aldolase, Biochemistry 32 (1993) 4685–4692.
[16] S.V. Benevolensky, D. Clifton, D.G. Fraenkel, The effect of increased phosphoglucose isomerase on glucose metabolism in *Saccharomyces cerevisiae*, J. Biol. Chem. 269 (1994) 4878–4882.
[17] J. Ovádi, P.A. Srere, Metabolic consequences of enzyme interactions, Cell Biochem. Funct. 14 (1996) 249–258.
[18] E.K. Pye, Biochemical mechanisms underlying the metabolic oscillations in yeast, Can. J. Bot. 47 (1969) 271–285.
[19] A.K. Ghosh, B. Chance, E.K. Pye, Metabolic coupling and synchronization of NADH oscillations in yeast cell populations, Arch. Biochem. Biophys. 145 (1971) 319–331.
[20] J. Wolf, R. Heinrich, Dynamics of two-component biochemical systems in interacting cells; synchronization and desynchronization of oscillations and multiple steady states, Biosystems 43 (1997) 1–24.
[21] M. Bier, B.M. Bakker, H.V. Westerhoff, How yeast cells synchronize their glycolytic oscillations: a perturbation analytic treatment, Biophys. J. 78 (2000) 1087–1093.
[22] J. Wolf, J. Passarge, O.J.G. Somsen, J.L. Snoep, R. Heinrich, H.V. Westerhoff, Transduction of intracellular and intercellular dynamics in yeast glycolytic oscillations, Biophys. J. 78 (2000) 1145–1153.
[23] J. Wolf, R. Heinrich, Effect of cellular interaction on glycolytic oscillations in yeast: a theoretical investigation, Biochem. J. 345 (2000) 321–334.
[24] A.T. Winfree, The Geometry of Biological Time, Springer, New York, 1980.
[25] P.C. Matthews, R.E. Mirollo, S.H. Strogatz, Dynamics of a large system of coupled non-linear oscillators, Physica D 52 (1991) 293–331.
[26] H. Daido, Order function theory of macroscopic phase-locking in globally and weakly coupled limit-cycle oscillators, Int. J. Bifurcation Chaos 7 (1997) 807–829.
[27] M. Rizzi, M. Baltes, U. Theobald, M. Reuss, In vivo analysis of metabolic dynamics in *Saccharomyces cerevisiae*: II. mathematical model, Biotechnol. Bioeng. 55 (1997) 592–608.
[28] B. Wurster, F. Schneider, Kinetik der glucosephosphatisomerase (EC 5.3.1.9) aus hefe in vitro und ihre anwendung auf flußberechnungen durch die Gärungskette der anaeroben Hefezelle, Hoppe-Seyler's Z. Physiol. Chem. 351 (1970) 961–966.
[29] C.J. Barwell, B. Hess, Application of kinetics of yeast pyruvate kinase in vitro to calculation of glycolytic flux in the anaerobic yeast cell, Hoppe-Seyler's Z. Physiol. Chem. 353 (1972) 1178–1184.
[30] S. Danø, Glycolytic Oscillations in Yeast Cells, University of Copenhagen, http://theochem.ki.ku.dk/~cats/library.html, 1999
[31] F. Hynne, P.G. Sørensen, K. Nielsen, Quenching of chemical oscillations: general theory, J. Chem. Phys. 92 (1990) 1747–1757.
[32] P. Richard, B. Teusink, H.V. Westerhoff, K. van Dam, Around the growth phase transition *S. cerevisiae*'s make-up favours sustained oscillations of intracellular metabolites, FEBS Lett. 318 (1993) 80–82.
[33] B.D. Hassard, N.D. Kazarinoff, Y.-H. Wan, Theory and Applications of Hopf Bifurcation, Cambridge University Press, Cambridge, 1981.
[34] M. Ipsen, F. Hynne, P.G. Sørensen, Systematic derivation of amplitude equations and normal forms for dynamical systems, Chaos 8 (1998) 834–852.
[35] K. Nielsen, P.G. Sørensen, F. Hynne, Chaos in glycolysis, J. Theor. Biol. 186 (1997) 303–306.
[36] B. Teusink, J. Diderich, H.V. Westerhoff, K. van Dam, M.C. Walsh, Intracellular glucose in derepressed yeast cells consuming glucose is high enough to reduce the glucose transport rate by 50%, J. Bacteriol. 180 (1998) 556–561.
[37] J.-U. Becker, A. Betz, Membrane transport as controlling pacemaker of glycolysis in *Saccharomyces Carlsbergensis*, Biochim. Biophys. Acta 274 (1972) 584–597.
[38] K.H. Kreuzberg, A. Betz, Amplitude and period length of yeast NADH oscillations fermenting on different sugars in dependence of growth phase, starvation and hexose concentration, J. Interdiscip. Cycle Res. 10 (1979) 41–50.
[39] A. Betz, R. Hinrichs, Incorporation of glucose into an insoluble polyglycoside during oscillatory controlled glycolysis in yeast cells, Eur. J. Biochem. 5 (1968) 154–157.
[40] W. De Koning, K. van Dam, A method for the determination of changes of glycolytic metabolites in yeast on a

subsecond timescale using extraction at neutral pH, Anal. Biochem. 204 (1992) 118–123.
[41] B. Chance, G. Williamson, I.Y. Lee, et al., Synchronization phenomena in oscillations of yeast cells and isolated mitochondria, in: B. Chance, E.K. Pye, A. Ghosh, B. Hess (Eds.), Biological and Biochemical Oscillators, Academic Press, New York, 1973.
[42] M.A. Aon, S. Cortassa, H.V. Westerhoff, K. van Dam, Synchrony and mutual stimulation of yeast cells during fast glycolytic oscillations, J. Gen. Microbiol. 138 (1992) 2219–2227.
[43] B. Hess, A. Boiteux, Substrate control of glycolytic oscillations, in: B. Chance, E.K. Pye, A. Ghosh, B. Hess (Eds.), Biological and Biochemical Oscillators, Academic Press, New York, 1973.
[44] M. Rizzi, U. Theobald, E. Querfurth, T. Rohrhirsch, M. Baltes, M. Reuss, In vivo investigations of glucose transport in *Saccharomyces cerevisiae*, Biotechnol. Bioeng. 49 (1996) 316–327.
[45] J. Cai, M. Pietzsch, U. Theobald, M. Rizzi, Fast purification and kinetic studies of the glycerol-3-phosphate dehydrogenase from the yeast *Saccharomyces cerevisiae*, J. Biotechnol. 49 (1996) 19–27.
[46] W.W. Cleland, The kinetics of enzyme-catalyzed reactions with two or more substrates or products, Biochim. Biophys. Acta 67 (1963) 104–137.
[47] B.L. Clarke, Stability of complex reaction networks, in: I. Prigogine, S.A. Rice (Eds.), Adv. Chem. Phys., vol. 43, Wiley, New York, 1980, p. 1.
[48] E. Mihaliuk, H. Skødt, F. Hynne, P.G. Sørensen, K. Showalter, Normal modes for chemical reactions from time series analysis, J. Phys. Chem. 103 (1999) 8246–8251.
[49] M.K. Jain, R.C. Wagner, Introduction to Biological Membranes, Wiley, New York, 1980.
[50] W.H. Press, B.P. Flannery, S.A. Teukolsky, W.T. Vetterling, Numerical Recipes in Pascal, Cambridge University Press, Cambridge, 1989.
[51] J.H. Wilkinson, C. Reinsch, Handbook for Automatic Computation, Springer, New York, 1971.
[52] P.G. Sørensen, CHEM, University of Copenhagen, 1999
[53] S.D. Cohen, A.C. Hindmarsh, CVODE, http://www.netlib.org/, 1994
[54] M. Marek, I. Schreiber, Chaotic Behavior of Deterministic Dissipative Systems, Cambridge University Press, Cambridge, 1995.
[55] M. Ipsen, I. Schreiber, Dynamical properties of chemical systems near Hopf bifurcation points, Chaos 10 (2000) 791–802.
[56] C.F. Bernasconi, Relaxation Kinetics, Academic Press, New York, 1976.
[57] T. Chevalier, I. Schreiber, J. Ross, Towards a systematic determination of complex reaction mechanisms, J. Phys. Chem. 97 (1993) 6776–6787.
[58] J.D. Stemwedel, I. Schreiber, J. Ross, Formulation of oscillatory reaction mechanisms by deduction from experiment, Adv. Chem. Phys. 89 (1995) 327–389.
[59] A. Brøndsted, An Introduction to Convex Polytopes, Springer, New York, 1983.
[60] Y. Kuramoto, Chemical Oscillations, Waves, and Turbulence, Springer, New York, 1984.
[61] M. Ipsen, F. Hynne, P.G. Sørensen, Amplitude equations for reaction diffusion systems with a Hopf bifurcation and slow real modes, Int. J. Bifurcation Chaos 7 (1997) 1539–1554.
[62] R.E. Viola, F.M. Raushel, A.R. Rendina, W.W. Cleland, Substrate synergism and the kinetic mechanism of yeast hexokinase, Biochemistry 21 (1982) 1295–1302.
[63] F. Azam, A. Kotyk, Glucose-6-phosphate as regulator of monosaccharide transport in baker's yeast, FEBS Lett. 2 (1969) 333–335.
[64] A. Kotyk, Mobility of the free and of the loaded monosaccharide carrier in *Saccharomyces cerevisiae*, Biochim. Biophys. Acta 135 (1967) 112–119.
[65] R.K. Crane, Hexokinases and pentokinases, in: P.D. Boyer, H. Lardy, K. Myrbäck (Eds.), The Enzymes, Academic Press, New York, 1962.
[66] E. Kopetzki, K.-D. Entian, Glucose repression and hexokinase isoenzymes in yeast, Eur. J. Biochem. 146 (1985) 657–662.
[67] E.A. Barnard, Hexokinases from yeast, Methods Enzymol. 42 (1975) 6–20.
[68] R. Fernández, P. Herrero, F. Moreno, Inhibition and inactivation of glucose-phosphorylating enzymes from *Saccharomyces cerevisiae* by D-xylose, J. Gen. Microbiol. 131 (1985) 2705–2709.
[69] BRENDA, On-line database at http://www.brenda.uni-koeln.de.
[70] R.N. Goldberg, Y.B. Tewari, Thermodynamics of enzyme-catalysed reactions: part 5. Isomerases and ligases, J. Phys. Chem. Ref. Data 24 (1995) 1765–1801.
[71] R.N. Goldberg, Thermodynamics of enzyme-catalysed reactions: part 6. Update, J. Phys. Chem. Ref. Data 28 (1999) 931–965.
[72] R.N. Goldberg, Y.B. Tewari, Thermodynamics of enzyme-catalysed reactions: part 4. Lyases, J. Phys. Chem. Ref. Data 24 (1995) 1669–1698.
[73] T.E. Barman, Enzyme Handbook, Springer, New York, 1969.
[74] W.K.G. Krietsch, Triosephosphate isomerase from yeast, Methods Enzymol. 41B (1975) 434–438.
[75] L.D. Byers, Glyceraldehyde-3-phosphate dehydrogenase from yeast, Methods Enzymol. 89 (1982) 326–335.
[76] R.N. Goldberg, Y.B. Tewari, D. Bell, K. Fazio, J. Anderson, Thermodynamics of enzyme-catalysed reactions: part 1. Oxidoreductases, J. Phys. Chem. Ref. Data 22 (1993) 515–582.
[77] A. Aust, S.-L. Yun, C.H. Suelter, Pyruvate kinase from yeast (*Saccharomyces cerevisiae*), Methods Enzymol. 42 (1975) 176–182.
[78] C.J. Dickenson, F.M. Dickinson, Some properties of an alcohol dehydrogenase partially purified from baker's yeast grown without added zinc, Biochem. J. 153 (1976) 309–319.

[79] F.M. Dickinson, G.P. Monger, A study of the kinetics and mechanism of yeast alcohol dehydrogenase with a variety of substrates, Biochem. J. 131 (1973) 261–270.
[80] A.J. Ganzhorn, D.W. Green, A.D. Hershey, R.M. Gould, B.V. Plapp, Kinetic characterization of yeast dehydrogenases, J. Biol. Chem. 262 (1987) 3754–3761.
[81] J. Albertyn, A. van Tonder, B.A. Prior, Purification and characterization of glycerol-3-phosphate dehydrogenase of *Saccharomyces cerevisiae*, FEBS Lett. 308 (1992) 130–132.
[82] S. Danø, F. Hynne, P.G. Sørensen, Dynamics of yeast cell populations. Proceedings of the Fifth International Conference on Fundamental and Applied Aspects of Physical Chemistry, Belgrade, Yugoslavia, 2000.